AD-A044 684   COLD REGIONS RESEARCH AND ENGINEERING LAB HANOVER N H   F/G 8/7
INVESTIGATION OF AN AIRBORNE RESISTIVITY SURVEY CONDUCTED AT VE--ETC(U)
AUG 77 S A ARCONE

UNCLASSIFIED   CRREL-77-20   NL

| OF |
ADA
044684
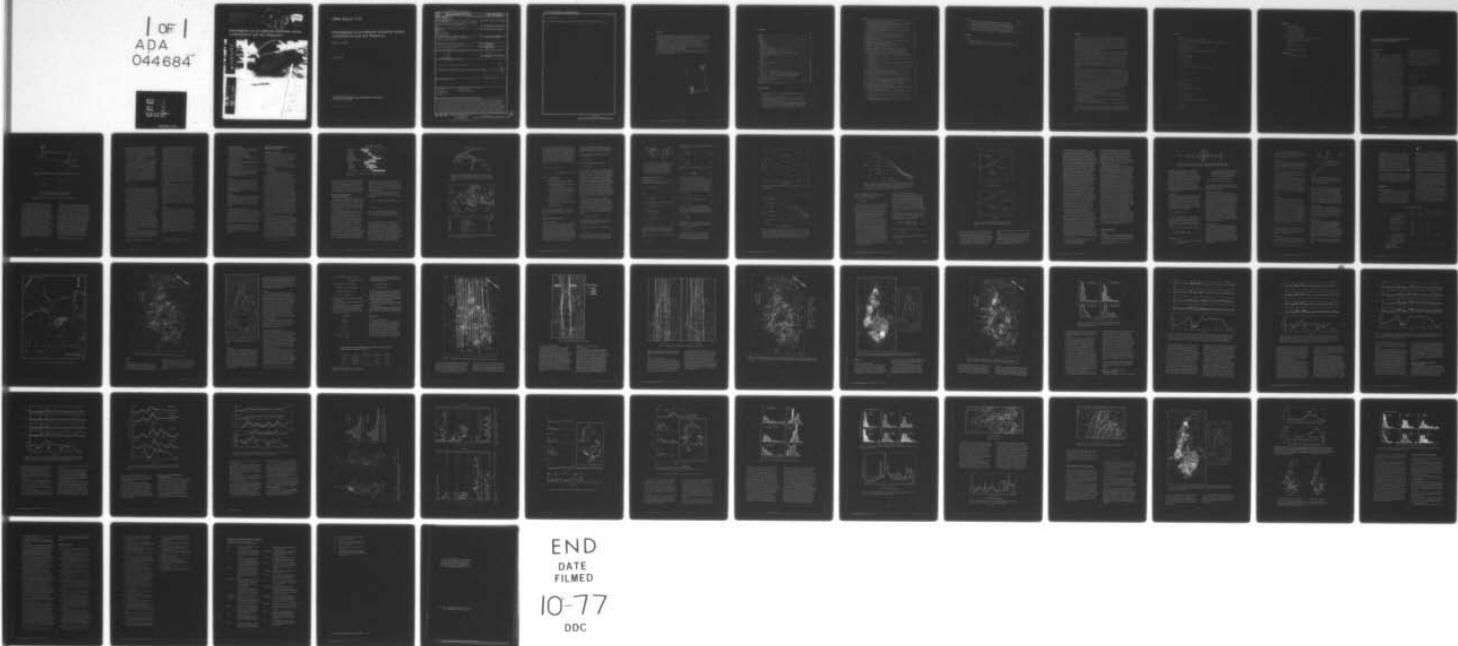
END
DATE
FILMED

10-77
DDC

CRREL
REPORT 77-20

SEP 30

CRREL

Investigation of an airborne resistivity survey conducted at very low frequency

ADA044684

AD No.
DDC FILE COPY

CRREL Report 77-20

Investigation of an airborne resistivity survey conducted at very low frequency

Steven A. Arcone

August 1977

REPORT DOCUMENTATION PAGE		READ INSTRUCTIONS BEFORE COMPLETING FORM
1. REPORT NUMBER CRREL Report 77-20	2. GOVT ACCESSION NO.	3. RECIPIENT'S CATALOG NUMBER
4. TITLE (and Subtitle) INVESTIGATION OF AN AIRBORNE RESISTIVITY SURVEY CONDUCTED AT VERY LOW FREQUENCY.		5. TYPE OF REPORT & PERIOD COVERED
		6. PERFORMING ORG. REPORT NUMBER
7. AUTHOR(s) Steven A. Arcone		8. CONTRACT OR GRANT NUMBER(s)
9. PERFORMING ORGANIZATION NAME AND ADDRESS U.S. Army Cold Regions Research and Engineering Laboratory Hanover, New Hampshire 03755		10. PROGRAM ELEMENT, PROJECT, TASK AREA & WORK UNIT NUMBERS
11. CONTROLLING OFFICE NAME AND ADDRESS U.S. Army Cold Regions Research and Engineering Laboratory Hanover, New Hampshire 03755		12. REPORT DATE August 1977
		13. NUMBER OF PAGES 57
14. MONITORING AGENCY NAME & ADDRESS(if different from Controlling Office)		15. SECURITY CLASS. (of this report) Unclassified
		15a. DECLASSIFICATION/DOWNGRADING SCHEDULE

16. DISTRIBUTION STATEMENT (of this Report)

Approved for public release; distribution unlimited.

17. DISTRIBUTION STATEMENT (of the abstract entered in Block 20, if different from Report)

18. SUPPLEMENTARY NOTES

19. KEY WORDS (Continue on reverse side if necessary and identify by block number)

Aerial surveys	Structural geology
Allagash, Maine	Subsurface investigations
Electrical resistivity	
Geophysics	

20. ABSTRACT (Continue on reverse side if necessary and identify by block number)

An airborne survey of earth electrical resistivity, computed from the complex tilt of the electric field vector of a VLF (17.8 kHz) radio surface wave, has been studied. The survey was conducted at a 150-m mean flight altitude. The bedrock of the survey area was slate containing an igneous stock. Topography was found to distort the resistivity contours through its effect upon the vertical component of the electric field. At 300-m flight altitude most resistivity information was retained due to the deterioration of topographic influence. The phase of the tilt, which cannot be distinguished from the amplitude by an airborne antenna system, was determined from a ground survey of the surface impedance and was found to be an important influence on the airborne detection of high resistivity areas. The entire 150-m survey was reevaluated with topographic effects removed. The resolution of the igneous

20. Abstract (cont'd)

geology improved and several of these improvements were verified by the ground measurements.

PREFACE

This report was prepared by Dr. Steven A. Arcone, Geophysicist, of the Physical Sciences Branch, Research Division, U.S. Army Cold Regions Research and Engineering Laboratory, as one of the requirements for his doctoral degree from Dartmouth College. The report was technically reviewed by Professor Bengt Sonnerup and Dr. Pieter Hoekstra.

The author would like to express his appreciation to: Professor Bengt Sonnerup and Dr. Pieter Hoekstra for their guidance and suggestions concerning this research, Dean Carl Long and Paul V. Sellmann for their support, and in particular, Allan Delaney for his efforts in data-processing and general assistance.

The contents of this report are not to be used for advertising or promotional purposes. Citation of trade names does not constitute an official endorsement or approval of the use of such commercial products.

iii

CONTENTS

ILLUSTRATIONS

SUMMARY

An airborne survey of earth electrical resistivity, computed from the complex tilt of the electric vector of a VLF (very low frequency) surface electromagnetic wave, has been studied. The survey was analyzed for the effects of topography vs resistivity, altitude, and wavetilt phase and amplitude. These factors can seriously affect the geologic resolution of this type of survey. Topographic relief affects at least one electric field component, flight altitude often varies over relief, and phase, which cannot be separated from amplitude by an airborne antenna system, is also quite variable when the earth's resistivity is stratified or when displacement currents are dominant.

A mountainous area in northern Maine was selected for study. The geology and topography of the area had been previously mapped and the area was within the surface wave range of the transmitter used (NAA, Cutler, Maine — 17.8 kHz). A standard wavetilt survey was then conducted at 150-m mean flight altitude. Resistivity effects upon the wavetilt field components were separated from those of topography by increasing the altitude of specific flight paths. The effect of altitude upon geologic resolution and the mean measured resistivity level were studied by repeating part of the standard survey at a higher altitude. The influence of phase and amplitude upon the measured airborne wavetilt was analyzed using the results of a ground survey of the total, complex surface impedance of the same radiowaves.

The results provided the following information. The igneous rock areas generally contained more high resistivity anomalies than did the slate areas. Without exception, all these anomalies fell on mountain flanks. The low resistivity areas (ponds) were strongly affected by the neighboring high resistivity areas. At altitudes above 300 m, large resistivity responses remained in the horizontal electric field but not in the vertical electric field. A topographic reevaluation, based on an adjustment of all values of the vertical electric field to the strength measured over areas of no relief, improved the geologic resolution of the profiles and of the contouring. The repeated standard survey at 300 m retained most of the geologic resolution of the 150-m standard survey. The ground values of apparent resistivity and phase showed that the slate areas were of comparable resistivity to the igneous areas but of much lower phase. They also showed that mountain ridges were comparable to flanks in airborne apparent resistivity when evaluated by the topographically corrected method.

Some of the conclusions reached were as follows:

1. The response of the vertical electric field to changes in resistivity is negligible compared with the response of the horizontal electric field to these same changes.

2. Topography primarily affects the vertical electric field, causing high resistivity zones to appear concentrated on flanks.

3. The phase of the wavetilt is an important factor for distinguishing high resistivity areas in regions of near-surface crystalline bedrock.

4. Resistivity anomalies less than twice the survey altitude in dimension were difficult to detect.

5. The quality of a survey may improve when conducted at an altitude at which topography does not affect the vertical electric field and will improve at standard altitudes when all values of the vertical electric field are adjusted to the measured strength over areas of no relief.

SYMBOLS

A	attenuator setting
α	plane wave angle of incidence upon ionosphere
γ	angle between azimuth of flightline and azimuth from center of survey to the transmitter
C_m	ionospheric focusing factor
d	groundwave propagation distance
Δd	propagation distance differential between sky and ground mode
δ	skin depth
E	electric field strength
E_0	reference field strength
E_1	initial field strength
ϵ	dielectric permittivity
F	Sommerfeld attenuation function
$F_{t,r}$	transmit/receive ground modification to antenna directivity
f	frequency
G	antenna directivity gain factor
H	magnetic field
i	$\sqrt{-1}$
κ	relative permittivity
λ	wavelength
μ	magnetic permeability
n	index of refraction
R_m	ionospheric reflection coefficient
ρ	resistivity
t	layer thickness
ϕ	phase of either W or Z_s
x, y, z	Cartesian coordinates
ψ	plane wave grazing angle of incidence upon earth
W	wavetilt
ω	radian frequency
Z	impedance

Subscripts

a	apparent, airborne
cal	calibrated value of a quantity
i	in-phase value of a quantity
m	number of sky wave hops
meas	measured value of a quantity
o	free space value of a quantity unless otherwise indicated
q	quadrature phase value of a quantity
r	receive
s	surface value of quantity
t	transmit
x, y, z	components of a vector quantity

Superscripts

'	topographically corrected quantity

INVESTIGATION OF AN AIRBORNE RESISTIVITY SURVEY CONDUCTED AT VERY LOW FREQUENCY

Steven A. Arcone

INTRODUCTION

Background

Geophysical methods are often used for the subsurface exploration of new sources of raw materials. These methods utilize the physical properties of rocks, sediments or certain minerals as a basis for the differentiation or identification of material. To evaluate these properties, the response of a particular system is usually compared to that of a simulated model of idealized geometry and material properties. Since ideal conditions are rarely encountered, however, further investigation of present techniques in nonideal environments and development of new techniques are needed.

Geophysical exploration often uses the physical property of electrical resistivity to differentiate material types. Materials important to the construction industry, such as sands, gravels and certain crystalline rocks, can exhibit resistivities one to two orders of magnitude greater than those of the more common materials with which they may be found. Sands and gravels are usually sought in areas of formerly existing deltas and floodplains, where the usual geological layering and a lack of topographic relief often conform to the geometric idealizations of mathematical models used for data comparison. Crystalline rocks, however, are usually associated with nonideal mountainous terrain. Therefore, before large amounts of time and money are invested in the exploration for crystalline rocks using a geophysical technique based on an idealized flat earth theory, careful investigation should be made of the response of that technique to the topographic conditions expected. In this report, the performance of an airborne resistivity exploration technique over a topographically complex region is experimentally analyzed.

The geophysical technique discussed uses radiowaves propagated from distant transmitters in regular use. The field vectors of these waves over homogeneous earth are shown in Figure 1a. In this figure, E_x is the electric field component tangential to the earth's surface and oriented toward the transmitter, E_z is the vertical electric field component, and H_y is the magnetic field component, also tangential to the earth's surface. Beneath the surface the large refractive index of the earth allows only E_x and H_y to exist, as the wave propagates vertically downward while attenuating exponentially. The quantities related to the resistivity of the earth are the surface impedance Z_s defined as

$$Z_s = \frac{E_x}{H_y}$$

and the wavetilt W defined as

$$W = \frac{E_x}{E_z} .$$

Generally, both these quantities convey the same information and either one or the other is measured. Since antennas can be used to measure these fields, the contact resistance problems of conventional galvanic techniques that use earth contact electrodes are avoided.

Both Z_s and W are complex quantities whose amplitudes and phases contain resistivity information. The mathematical theory of plane waves incident upon a "flat" earth (i.e. with topographic relief dimensions that are a small fraction of the wavelength used) containing horizontal, homogeneous layers (Cagniard 1953) is the basis for converting Z_s or W into resistivity and, ultimately, geological information. An "apparent resistivity" ρ_a, usually expressed in ohm-meters and derived from either $|Z_s|^2$ or $|W|^2$ is most commonly determined. At any particular frequency ρ_a represents some sort of average for the layering to a depth which increases with decreasing frequency.
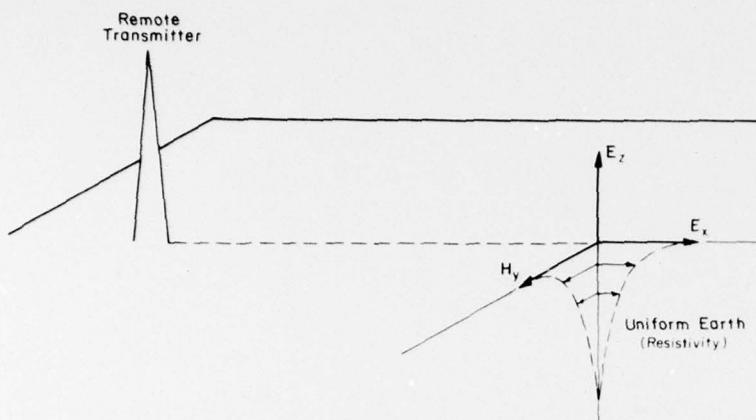
a. Field vectors above homogeneous earth shown refracting vertically into the ground.
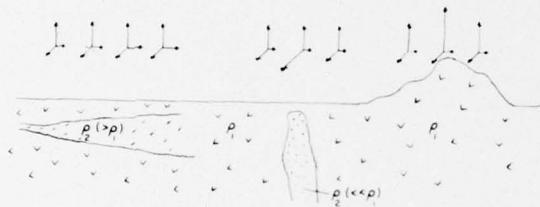
b. Major VLF field changes known to take place when local changes in earth conditions are encountered.

Figure 1. Electromagnetic field vectors of a radiowave propagating over the earth's surface.

Ideally, then, many frequencies could be used to analyze a resistivity stratification. Practically, however, only transmitters operating in the VLF band (very low frequency, 10-30 kHz or 10-30 km wavelength) are powerful enough to allow their radiation to be used worldwide. When radiation at higher frequencies is available, the information provided is usually more difficult to interpret because of the undesirable effect of displacement currents. Transmitters at lower frequencies do not exist; therefore, natural sources of radiation in the ELF (extremely low frequency, $1-10^3$ Hz) and in the ULF (ultra low frequency, $10^{-3}-1$ Hz) bands are used. The primary sources within this range are atmospheric electric discharges and diurnal variations in the earth's magnetic field caused by solar emission, ionospheric emission, etc. The use of this radiation is known as the magnetotelluric (MT) method (Keller and Frischknecht 1966, Telford et al. 1976). In this report, attention will be confined to only VLF.

Observed VLF responses to local changes in an earth environment are depicted in Figure 1b. The incident wave may be a surface wave* or a sky wave at grazing incidence. E_x is primarily affected over gradual horizontal changes in earth resistivity (Hoekstra et al. 1974) so as to maintain continuity of current flow in the x direction. H_y is primarily affected over large lateral discontinuities such as highly conductive ore-bearing dikes (Paal 1965, 1968) in which strong eddy currents may be induced. E_z is primarily affected over large topographic disturbances (Harrison et al. 1971), an electrostatic effect related to the mountain geometry and therefore occurring independently of the value of earth resistivity. It therefore violates the important assumption of a flat earth used in the mathematical theory employed for resistivity data reduction.

All the above responses are generally oversimplified because changes in one field component must be

_____

* Also referred to as a ground wave in the literature.

2

accompanied by changes in all other field components as predicted by Maxwell's equations. However, to date, no studies have been made to demonstrate that topographic effects can be separated from resistivity effects for any VLF field component. Consequently, resistivity is presently computed from the ratio of E_x to E_z or to H_y as measured in-situ.

Presently, Z_s is commonly measured at ground level because vegetation interferes with E_z. Commercially available instruments are capable of measuring amplitude and phase, and they employ H_y as the phase reference. At airborne levels, above vegetative influence, only the imaginary or quadrature value of the complex wavetilt* $W_q = E_{xq}/E_{zi}$ provides meaningful information (E_z is used as the phase reference). The reasons for this will be discussed later, but it is important to realize now that amplitude $|W|$ and phase angle ϕ of W cannot be separated by an airborne system, since W_q is related to both quantities by the relation:

$$W_q = |W| \sin \phi.$$

Therefore, in an airborne survey, it is entirely plausible that a very large amplitude of W caused by a very resistive material may remain entirely undetected because of a low value of ϕ, such as occurs when resistivity rapidly increases with depth or when dielectric properties become important. Also, during an airborne survey, an aircraft often changes flight altitude by several hundred meters when navigating over steep relief. This in itself must alter the geologic resolution of a survey.

Some compensation for the phase effect is presently made in the data processing by assuming that ϕ is usually near $45°$ (Barringer 1972, 1973), as with homogeneous ground where $W_i = W_q$ and the true resistivity can be determined. Unfortunately, homogeneity is not common over the depths capable of being penetrated by VLF radiation. Although Keller et al. (1970) and Hoekstra et al. (1974) have assumed that $45°$ is probably correct over exposed, deep-rooted bedrock formations because such geology itself is reasonably homogeneous, Sellmann et al. (1975) have reported Z_s phase values as low as $13°$ over exposed deep crystalline formations. Should this phase hold true for W, then these observations would contradict the $45°$ phase assumption for such formations.

Many airborne resistivity surveys have been made in North America. Over areas of minor topographic relief, they have usually been successful in delineating regions of permafrost (Hoekstra et al. 1975, Geological Survey

of Canada 1973) and in detecting intertill gravel deposits (Culley et al. 1975). All verifications have been made by ground reconnaissance, and in the work of Hoekstra et al. (1974, 1975) ground measurements of Z_{sq} were successfully related to the airborne measurements of W_q, although some of the finer detail of the ground readings did not appear in the airborne results.

Of the few surveys known to have been conducted over regions of more severe topographic relief, none has been adequately verified by ground reconnaissance. Keller et al. (1970) investigated granitic formations in Colorado, but did not have VLF equipment available for ground resistivity verification. Both Sellmann et al. (1974) and Hoekstra et al. (1975) conducted surveys over mountainous regions in interior Alaska in an attempt to delineate permafrost, but made no ground observations to verify their conclusions. An examination of the original data of Hoekstra et al. (1975) by the author revealed the same topographic sensitivity of E_z as did the observations by Harrison et al. (1971) mentioned above.

In summary, large deposits of needed raw materials often lie in mountainous regions. Since these deposits are usually of exceptionally high electrical resistivity, a VLF airborne wavetilt survey would seem ideally suited for discovering them. However, the results of previous investigations have shown that three basic assumptions used in VLF data processing — a flat earth, $45°$-phase angles over crystalline bedrock geology, and a steady flight altitude — can be seriously violated. Consequently, further investigation is needed into the performance of the VLF survey system in mountainous terrain.

Objectives

The experimental objectives were to determine the effects of: 1) topography vs resistivity, 2) flight altitude,[†] 3) amplitude of the wavetilt, and 4) phase of the wavetilt upon the geologic resolution of a standard airborne wavetilt survey conducted at very low frequency. Based on previous experiments by Harrison et al. (1971), it was expected that topography would severely affect E_{zi}, but it had not been shown either experimentally or theoretically whether topography would affect E_{xq} or whether changes in resistivity would affect E_{zi}. Nor had the separate influences of amplitude and phase upon the airborne wavetilt been investigated for an actual survey. The effect of flight altitude also had not been investigated.

---

* q and i refer to quadrature and in-phase components, respectively.

† In this report the term "flight altitude" denotes elevation above terrain and not above sea level.

3

Experimental procedures

In the experiments performed, a mountainous area in northern Maine was selected for study. The area was chosen for the following reasons:

1) the topography was mapped

2) the bedrock geology was mapped

3) the overburden was usually less than 1 m with common outcrops

4) the site was within the surface wave range of the transmitter used, and therefore the radiation was free of ionospheric interference

5) apparent resistivity and phase contrasts were known to exist at VLF.

The area was surveyed at VLF using standard airborne wavetilt and data processing techniques. The survey results were then analyzed as follows to meet the objectives previously mentioned.

Topography

The mean altitude of specific flight paths that traversed the steepest relief was varied to eliminate topographic effects upon the field components. The responses at the higher altitudes provided information as to which field components were responsive to resistivity changes and, hence, which were responsive to topographic changes.

Flight altitude

The effect of flight altitude upon geologic resolution and mean apparent resistivity level was studied by narrowing the flightline spacing of part of the standard survey and then repeating it at twice its mean flight altitude. The two surveys were then contoured and compared.

Amplitude and phase of the wavetilt

These factors were investigated simultaneously by comparing apparent resistivities obtained from a ground survey of the total complex surface impedance to those obtained from the airborne wavetilt. It was expected that H_v would generally be in phase with E_z making this procedure valid. As will be shown, E_z and H_v were generally in phase and H_v was unaffected by topography.

The information gained from the high-altitude flights justified a topographic correction scheme which was devised and applied to the original survey. Some of the corrections were verified by the results of the ground survey.

PRINCIPLES OF ELECTROMAGNETIC RESISTIVITY SURVEYING

Resistivity of earth materials

The physical property of electrical resistivity is the basis of electromagnetic resistivity surveying for subsurface exploration. Resistivity values of most earth materials usually fall between 10 and 10,000 ohm-m. The most important factors that determine the resistivity of unfrozen crustal materials are

1. Intrinsic resistivity of the constituent minerals.

2. Textural properties such as grain size, porosity and permeability.

3. Water content.

4. Ionic concentration in free water.

5. Ionic concentration in adsorbed water.

Factor 1 is usually insignificant for most materials. Common minerals such as micas and quartz have resistivities greater than 10^{10} ohm-m (Parkomenkho 1967). Ore minerals (e.g. metallic oxides and sulfides) are much more conductive but are volumetrically insignificant in most materials. Clay minerals (e.g. montmorillonite and kaolinite) warrant the most important mineralogical consideration when discussing resistivity factors. The large amount of ions usually adsorbed on the crystal lattice of clays (Grim 1953) produces a surface conduction effect that can appreciably lower the resistivity of a sediment or rock (Ward 1967).

Factors 2 through 5 commonly account for the resistivity values observed in earth materials. Conduction is mainly electrolytic and takes place along continuous films of water adsorbed on grain boundaries and also through water that may fill the pore spaces available (Parkomenhko 1967). Since conductivity (the inverse of resistivity) is proportional to the number of ions present and their mobility, the ionic concentration of the water and the number of conducting paths, as determined by the material's textural properties, are of utmost importance.

In Figure 2 the expected ranges of resistivity are compiled for most earth materials, based on past surveys and laboratory measurements. The unconsolidated materials, clay and marl* through loose sands, generally show an increase in resistivity with particle size. This may be expected from the corresponding decrease in available adsorbing surface area. Moraine or well-mixed glacial deposits exhibit a wide range of resistivities due to large variations in material type. The consolidated materials, chalk through crystalline rocks (e.g. granite, gneiss or schist), generally show an increase in resistivity with decreasing porosity and permeability. Clay content

---

* See glossary for definitions of geologic terms used.

RESISTIVITY (ohm-meters)
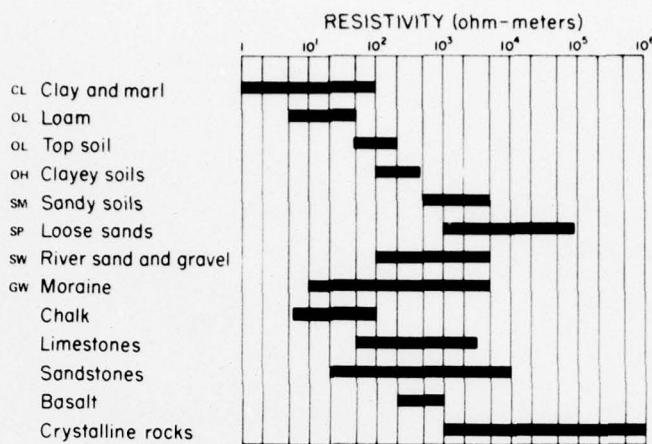
Figure 2. Resistivity ranges of most earth materials (after Culley et al. 1975).

may also be significant, as with sandstones (Ward 1967), and the large amounts of iron and magnesium rich minerals in basaltic igneous rocks can make them less resistive than granitic igneous types. In all cases, the effects of weathering, jointing or fracture may significantly lower the resistivity of the fresh rock due to increased permeability, formation of clay minerals, etc.

Radiowave propagation within the earth-ionosphere waveguide

Electromagnetic resistivity surveying utilizes radiowaves propagating within the earth-ionosphere waveguide. These waves propagate by two important modes which begin to form at a distance of about one wavelength from the antenna. Both modes will be considered because their relative ranges can affect the planning of a resistivity survey.

The two propagation modes, as radiated by a vertical electric dipole antenna situated at the earth's surface, are illustrated in Figure 3. The "surface wave" is so named because its field strength decays with height above the earth's surface. The "sky wave" is actually the sum of many modes formed between the ionosphere and the earth and exists at all frequencies below about 10^8 Hz. Both modes are transverse magnetic and their field vectors at the earth's surface may be represented as in the figure. E refers to the electric field components, H to the magnetic field component and x, y, and z to a local right-hand Cartesian coordinate system. z is perpendicular to the earth's surface and x and y are tangential. α and ψ, described below, refer to the incidence angles of the first order sky wave mode upon the ionosphere and earth, respectively.

As has been experimentally shown in a number of investigations reported by Hollingworth (1926) and by Alpert (1963), both modes do not necessarily combine in phase at the earth's surface. However, depending on distance from the transmitter, usually one or the other mode predominates.

The surface wave has less range than the sky wave and is relatively more important at distances of less than 400 km at VLF to the transmitter. At a distance d such that

$$d \leqslant 50/f^{1/3} \text{ miles (Jordan and Balmain 1968)} \quad (1)$$

or

$$d \leqslant 80/f^{1/3} \text{ km}$$

where f is in megahertz, Sommerfeld (1909), Weyl (1919) and Norton (1936) have shown that surface wave field strength is determined by the expression

$$E_z = E_t F/d \quad (2)$$

where E_z is the vertical electric field strength in V/m, E_t is the initial field strength, and F is known as the Sommerfeld attenuation function. F depends on the frequency, distance, and electrical properties of the earth, and graphs are available for finding its absolute value for both electric and magnetic dipole type antennas (Kraichman 1970). At VLF frequencies, the higher power of existing transmitters can allow the surface wave to extend to over 1000 km over sea water (Watt 1967).

Beyond about 800 km from the transmitter the sky wave predominates over resistive earth (Watt 1967).

5
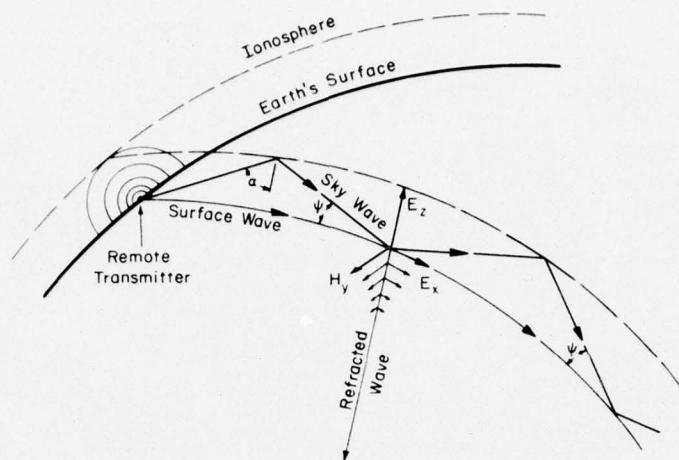
Figure 3. Two radiowave propagation modes in the earth-ionosphere waveguide (see text for explanation of symbols). The electromagnetic field components are characteristic of radiation from a vertical electric dipole.
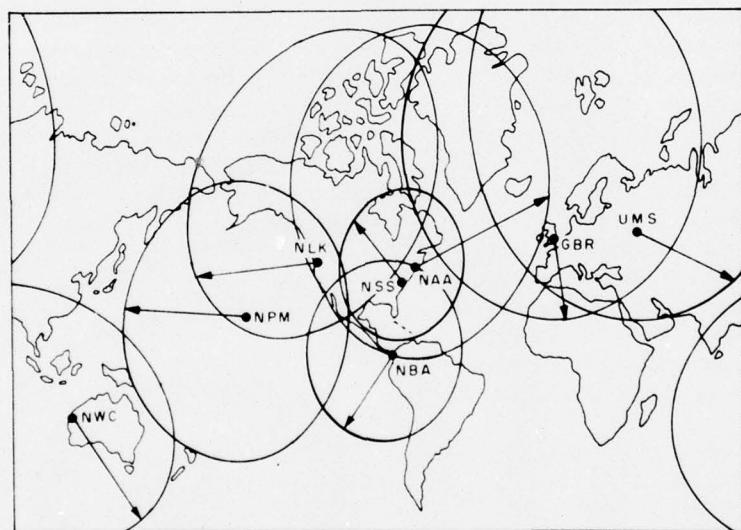
Call	Location	Frequency (kHz)
NAA	Cutler, Maine	17.8
NLK	Jim Creek, Washington	18.6
NSS	Annapolis, Maryland	21.4
NBA	Balboa, Canal Zone, Panama	24.0
GBR	Rugby, England	16.0
UMS	Gorky, USSR	17.15
NWC	Northwest Cape, Australia	23.3 and 15.5
NPM	Lualualei, Hawaii	23.4

Figure 4. Coverage for well-known VLF stations. Circles enclose approximate areas where field strengths exceed $100 \, \mu V/m$.

The sky wave may then be represented as the sum of incident and reflected traveling plane waves which combine to produce many standing wave modes between the ionosphere and the earth. Following Watt (1967), the total sky wave field at VLF may be given as the sum of all possible rays which may undergo one or more "hops" as illustrated in Figure 3. For a particular hop, the vertical electric field E_{zm} as transmitted and received by vertical dipoles at the earth's surface may be written as

$$E_{zm} = E_t G_t^{1/2} (\alpha, \psi) F_t R_m C_m F_r$$

$$\times \cos \psi \left(1 + \frac{\Delta d}{d}\right)^{-1} e^{-i(2\pi \Delta d/\lambda)} \quad (3)$$

where E_t = initial field strength
m = number of hops
α = angle of incidence upon the ionosphere measured from the vertical
ψ = angle of incidence upon the earth measured from the earth tangential
$G_t = \cos^2 \psi$ = antenna directivity gain factor
F_t = transmitting antenna field strength pattern modification produced by the proximity of a finitely conducting earth
F_r = same as F_t but for the receiving antenna
R_m = ionospheric reflection coefficient
C_m = ionospheric focusing factor
Δd = difference in length between the sky mode path and great circle arc between the transmitter and receiver
λ = free space wavelength.

At distances of less than 2000 km the single hop sky wave is the predominant mode. The effective range of most of the world's VLF transmitters is shown in Figure 4.

Radiowave interaction with the earth

General considerations

Not all radiowave energy of both the sky and surface waves is confined to the earth-ionosphere waveguide. A small fraction is refracted below the earth's surface, as represented in Figure 3. In the earth the energy is partly absorbed and partly scattered back to the surface from the subsurface layers of rocks and sediments. The depth of penetration increases with decreasing frequency, allowing values between 10^3 and 10^6 Hz to be ideally suited for exploring the composition of the first few hundred meters of the earth's crust. In this frequency range,

resistivity is the predominant electrical property that allows differentiation of material type, although permittivity may also be important as will be shown below.

These electrical properties can be related to the wavetilt W defined as

$$W = E_x/E_z \big|_{z=0} \quad (4)$$

and to the surface impedance Z_s defined as

$$Z_s = E_x/H_y \big|_{z=0} \quad (5)$$

where E_x and E_z are in V/m, H_y is in ampere-turns/meter and Z_s in ohms. These definitions automatically apply to the surface wave, but the sky wave's grazing angle of incidence ψ must be approaching $0°$ for these quantities to be useful. E_x need not be in phase with either E_z or H_y, making W and Z_s complex. Frischknecht (1973) has stated that the amplitudes and phases of these ratios for the sky wave at VLF are not affected by ionospheric events or by the total path of propagation from the transmitter, but that they are primarily determined by the local electrical properties at the point of measurement. Although this has not yet been verified by diurnal observations, the proximity of ψ to $0°$ at large distances, the extensive range of existing transmitters, and the deep earth penetration make VLF best suited for resistivity surveys.

The basic definitions used in electromagnetic resistivity surveying are adopted from the simply layered flat earth model shown in Figure 5. Often this model is not exactly applicable, but it has proven to be a useful guideline for data interpretation (Palacky et al. 1975, Nabetani and Rankin 1969). Below, some of the mathematical formulations will be reviewed. In this model we find $W = Z_s/Z_0$ where the free space impedance Z_0 is defined as

$$Z_0 = \sqrt{\mu_0/\epsilon_0} = 377 \text{ ohms}$$

with free space magnetic permeability, $\mu_0 = 4\pi \times 10^{-7}$ henry/meter and the free space electric permittivity $\epsilon_0 = 8.85 \times 10^{-12}$ farad/meter.

This result is obtained because as ψ approaches $0°$

$$E_z/H_y \to Z_0. \quad (6)$$

Therefore, for these cases, a measure of either W or Z_s will provide the same information. The derivation of the following formulas may be found in Wait (1962).

7
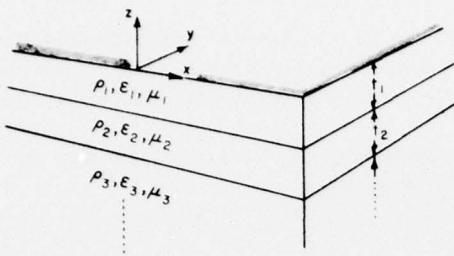
Figure 5. Simply layered flat earth model used for deriving the definitions of apparent resistivity (1-layer case) and also used in modern data interpretation techniques (3-layer case). The magnetic permeability μ is usually taken as equal to that of free space for each layer.

Homogeneous earth and definitions of apparent resistivity

When the electrical properties are uniform with depth, the surface impedance is given by

$$Z_s = -\frac{Z_0\sqrt{n^2 - 1}}{n^2} \qquad (7)$$

where

$$n = \sqrt{\kappa - \frac{i}{\rho\omega\epsilon_0}} \qquad (8)$$

is the refractive index of the earth. In this expression,

$\omega = 2\pi f$ (f = frequency in Hz)

$i = \sqrt{-1}$

κ = relative permittivity

ρ = resistivity in ohm-m.

The quantity α, defined as

$$\alpha = \frac{1}{\rho\omega\kappa_0} \qquad (9)$$

is a measure of the relative strengths of displacement and conduction currents and is usually much greater than unity at VLF and at resistivities less than 10^4 ohm-m.

For all practical cases $n \gg 1$ and eq 7 may be simplified to

$$Z_s = -Z_0/n. \qquad (10)$$

An apparent resistivity ρ_a is then defined from a measurement of Z_s as

$$\rho_a = \frac{|Z_s|^2}{\omega\mu_0} \qquad (11)$$

or of W as

$$\rho_a = \frac{|W|^2}{\omega\epsilon_0}. \qquad (12)$$

which equals the true resistivity when $\alpha \gg 1$. For such cases

$$Z_s = -(1 + i)\sqrt{\frac{\omega\mu_0\rho}{2}} \qquad (13)$$

and the phase angle ϕ of either Z_s or W is 45°.

For resistivity values below 10^4 ohm-m, $|W| < 0.12$ at VLF. Therefore, serious leakage of E_z into the horizontal antenna that measures E_x will occur when the antenna is mounted on an unstable platform as in an aircraft. In this case, since W and Z_s are complex quantities, only the component of E_x that is in quadrature phase with either E_z or H_y can be used. Using the wave-tilt as an example,

$$W = |W|(\cos\phi + i\sin\phi), \qquad (14)$$

so that W_q the quadrature wavetilt value is

$$W_q = |W|\sin\phi. \qquad (15)$$

A measurement of only W_q cannot distinguish the separate effects of amplitude and phase and a phase angle of 45° must be arbitrarily assumed. The formula for converting W_q to apparent resistivity, defined as ρ_q in this case, is

$$\rho_q = \frac{2|W_q|^2}{\omega\epsilon_0} \qquad (16)$$

which gives the correct value of resistivity for a homogeneous earth. When phases are different than 45°, ρ_q is related to ρ_a by the formula:

$$\rho_q = 2\rho_a \sin^2\phi. \qquad (17)$$

As was shown in Figure 3, the refracted waves propagate nearly vertically into the ground. The propagation factor for the fields within the earth is $\exp(i\sqrt{-i\omega\mu_0/\rho}\ z)$, which can be rewritten as

8
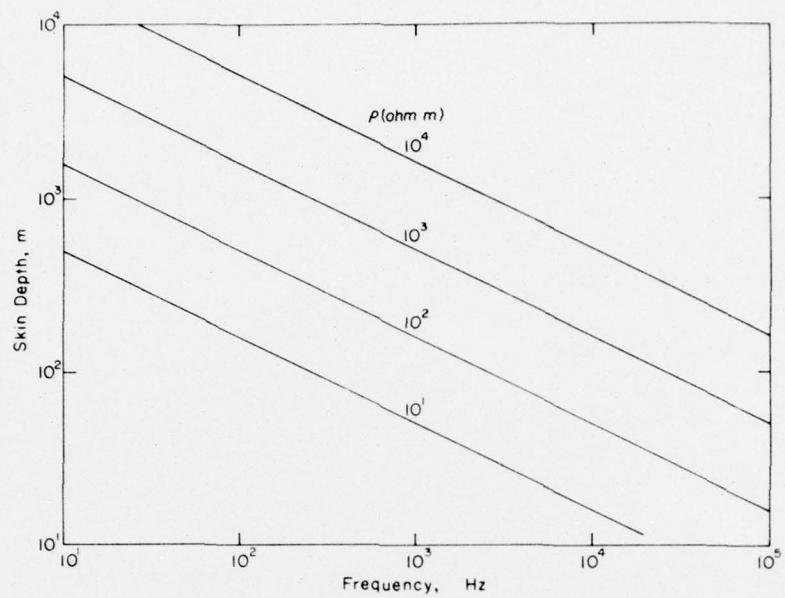
Figure 6. Skin depth of radiowaves as a function of frequency for various values of resistivity.
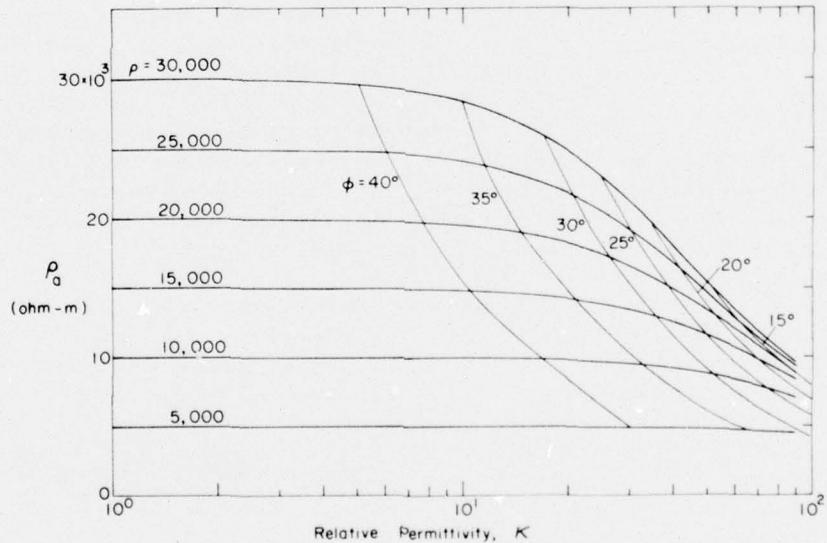
Figure 7. Apparent resistivity ρ_a and phase ϕ at 20 kHz for various homogeneous earth models of resistivity ρ and relative permittivity κ. Both ρ_a and ϕ decrease as κ increases. ϕ is plotted in equiphase contours and approaches $45°$ as κ approaches 1. At a value of $\kappa = 40$ and $\rho = 30,000$ ohm-m, an apparent resistivity of 18,000 ohm-m and a phase of about $20°$ will be determined from the Z_s or W method.

9
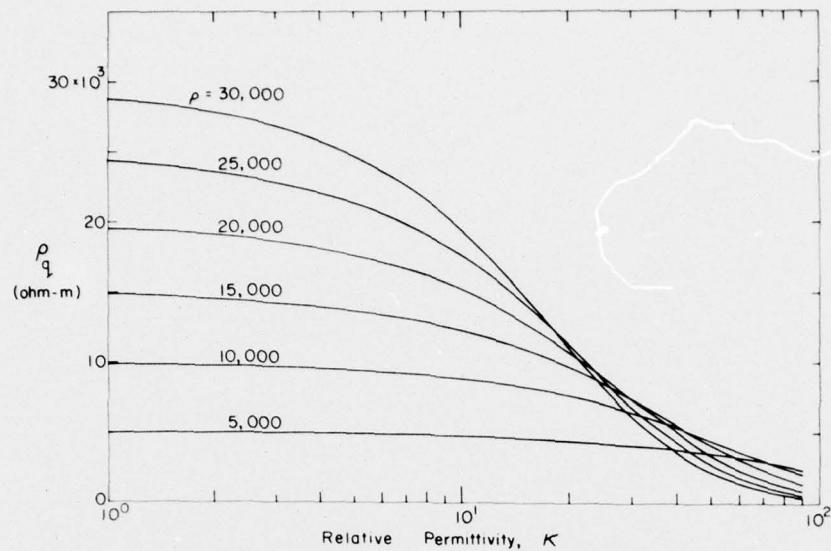
Figure 8. Quadrature value of apparent resistivity ρ_q (computed from eq 17) at 20 kHz for various homogeneous earth models of resistivity ρ and relative permittivity κ. At a value of $\kappa = 40$, an actual resistivity of 30,000 ohm-m will be measured by an airborne system as an apparent resistivity of about 2,500 ohm-m.

$\exp\left[(i+1)\sqrt{\omega\mu_0/2\rho}\ z\right]$ and is valid for $\alpha \gg 1$. A measure of the depth of penetration of the waves is then given by the skin depth formula:

$$\delta = \sqrt{2\rho/\omega\mu_0}\ , \qquad (18)$$

which is the depth at which the radiation will attenuate to e^{-1} of its original value at the surface. δ is plotted in Figure 6 as a function of frequency for various resistivities. Any change in the resistive properties of the earth below this depth will not produce any significant change in either the amplitude or phase of Z_s or W. When changes take place above this depth, then both amplitude and phase will be affected.

When $\alpha \approx 1$ or less, n of eq 8 tends toward a real quantity suppressing both phase and amplitude of Z_s and W. This is illustrated in Figure 7 for a frequency of 20 kHz in the VLF range. For fixed values of resistivity, the decreases in apparent resistivity and phase are plotted as a function of the increasing dielectric constant κ for various homogeneous earth models of resistivity ρ. The most seriously affected quantity is ρ_q of eq 17 which is plotted against the same variables in Figure 8. For a particular value of ρ, ρ_q decreases more rapidly with increasing κ than does ρ_a of Figure 7 due to the added phase factor. This is significant for airborne systems which only measure ρ_q. Values of $\kappa > 20$ are not uncommon for many crystalline rock types (Parkomenkho 1967).

Vertically stratified homogeneous layers

When earth consists of two or more layers of different thicknesses and electrical properties, W and Z_s will change in both magnitude and phase, depending upon all the earth parameters involved. Wait (1962) presents a simple method for generating the formulas for any number of layers, and present data processing generally uses a three-layer model (Palacky 1975), but only a two-layer case will be considered here. This case is sufficient to demonstrate some of the more important effects.

When the upper layer is characterized by a resistivity ρ_1 and depth t_1 and the semiinfinite lower layer has resistivity ρ_2 and $\alpha \gg 1$ for both layers, then the surface impedance is found from the formula:

$$Z_s = -\sqrt{i\omega\mu_0\rho_1}\ \frac{\sqrt{\rho_2/\rho_1} + i\tan k_1 t_1}{1 + i\sqrt{\rho_2/\rho_1}\tan k_1 t_1}\ , \qquad (19)$$

where the wave propagation number k_1 is defined as

$$k_1 = \sqrt{-i\omega\mu_0/\rho_1}\ .$$

An apparent resistivity is then defined in the manner of eq 11 and 12 as

$$\rho_a = \frac{|Z_s|^2}{\omega\mu_0} \qquad (20)$$

10
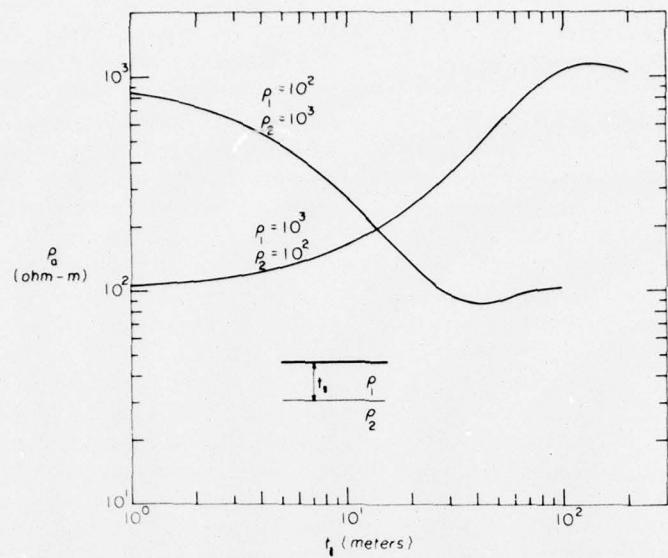
a. Apparent resistivity.
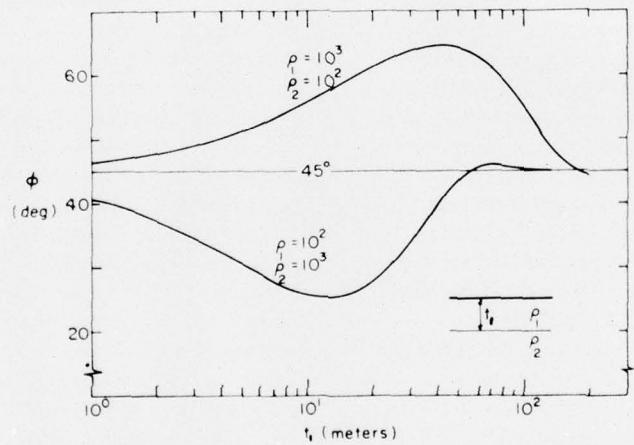
b. Phase.

Figure 9. The apparent resistivity (a) and phase (b) of two-layer earth models as a function of layer depth at a frequency of 20 kHz.

which is correct when t_1 becomes infinitely small. In Figure 9 are plotted the variations in apparent resistivity and phase for two-layer earth as a function of layer thickness at 20 kHz. When the upper layer is relatively more resistive, the phase angle lies between $45°$ and $90°$; when the upper layer is less resistive, the phase angle lies between $0°$ and $45°$. This phase behavior can be generalized for any resistive structure where the resistivity either progressively decreases or increases with depth.

When α of eq 9 is comparable to unity for the upper layer, and $\rho_1 > \rho_2$, the phase angles are strongly pushed toward $90°$ while decreasing the apparent resistivity. When α is comparable to unity for the lower layer and $\rho_2 > \rho_1$, the phases will strongly decrease toward $0°$ while also decreasing the apparent resistivity.

11

Irregular surface and subsurface conditions

Extreme mathematical difficulties arise in handling irregular conditions because of the mixed geometries that are always involved. Numerical techniques (Jones and Price 1970, Coggon 1971, Swift 1971) have been applied for studying the effect of lateral inhomogeneities (e.g. ore bearing dikes) upon plane waves, but these have been primarily at magnetotelluric frequencies below 10^3 Hz. At VLF Lytle (1975) and Hughes and Wait (1975) have investigated cases involving a flat earth with non-uniform layering. In particular, Hughes and Wait have investigated TM waves incident at values of ψ approaching $0°$. They demonstrate that both the phase and amplitude of Z_s and W qualitatively correlate with changes in subsurface layer dimensions that occur over distances far shorter than a free space or in-situ wavelength. However, their results also show that the phases of these two quantities are not necessarily the same, nor are $|W|$ and $|Z_s|$ always related by Z_0. Wait (1971) discusses similar "recovery" effects for ground waves and reviews the literature on this subject.

Layering interpretations of simultaneous measurements of ρ_q at two or more frequencies by an airborne wavetilt system* have been compared to the known geology over flat regions. Culley et al. (1975) successfully correlated the interpretation of ρ_q profiles taken at frequencies in the BCB,† LF** and VLF bands with drill hole results in layers of till and gravel in Saskatchewan, Canada. Hoekstra et al. (1975) demonstrated the sensitivity of both VLF and LF to changes in permafrost conditions in several study areas near Fairbanks, Alaska. An examination of Hoekstra's original data by this author revealed that at VLF E_z was far more stable than E_x over apparent resistivities ranging between about 100 and 4000 ohm-m.

Ground-based observations have been limited by the availability and portability of suitable equipment. Pioneering work in wavetilt measurements of ground electrical properties was done by Eliassen (1957), King (1968) and Blomquist (1970). However, extensive use of the wavetilt method for ground level geophysical surveying is limited by the interference of vegetation with E_z. Consequently, the surface impedance method, when used with a system developed by Collett and Becker (1967), has made extensive ground surveying possible at VLF. In Hoekstra's work mentioned above, airborne measurements of ρ_q derived from W_q were successfully compared to limited ground measurements of ρ_q derived from Z_s in areas of marginal relief by using

---

* For the earlier development of this system see Frischknecht (1971), Barringer (1972), McNeill et al. (1973).

† BCB: Broadcast Band, 500-1600 kHz.

** LF: Low Frequency, 200-400 kHz.

eq 17. Since the airborne measurements showed that E_z was stable, this implied that H_y was also stable. Thus, the relation of eq 6 was probably maintained, although plane wave sky mode theory (the transmitter was over 2400 km away) predicts changes in all components when ρ changes. Hoekstra's work therefore demonstrated that either ground or airborne resistivity mapping in regions of little relief is usually determined primarily by fluctuations in E_x.

Observations over topographically complex areas have been limited to VLF. Harrison et al. (1971), using antennas mounted below a helicopter, observed that the vertical electrical field (Station NAA, Cutler, Maine) can intensify over mountain ridges by more than 6 db (this effect was illustrated in Fig. 1), but that the effect disappears at flight altitudes comparable to the mountainous relief itself. Harrison theorized that this was an electrostatic effect (the mountain size is a small fraction of a VLF wavelength) and reproduced this same behavior by superimposing the field of an induced, hemispherical dipole model of the mountains observed upon the field of a VLF ground wave. Harrison used the same electrical parameters for all of his ground models. Sellmann et al. (1974) observed that high values of airborne resistivity were most prevalent in valley regions of a survey near Fairbanks, Alaska, and reasoned that this resulted from the presence of permafrost. A subsequent examination of these data revealed that the vertical field (Station NLK, Jim Creek, Washington) was enhanced over ridge tops as with Harrison's observations, thereby suppressing the apparent resistivity of the mountainous areas. These data also revealed that the horizontal field E_x was more consistent with known distributions of permafrost. Sellmann et al. (1975), using the surface impedance method over a variety of near-surface igneous and metamorphic rocks in areas of variable relief in northern Maine, reported a wide range in both apparent resistivity and phase. At apparent resistivity values between 4000 and 30,000 ohm-m, the phases ranged from $13°$ to $58°$. Phase values as low as $13°$ can seriously affect the ability of an airborne system to detect such high resistivity values, should these same phases hold true for the wavetilt.

INSTRUMENTATION

Airborne

The airborne E-Phase†† wavetilt system was used for the airborne surveys. In this system illustrated in Figure 10, horizontal and vertical electric dipole antennas are

---

†† E-Phase (Barringer Research Ltd., Toronto, Canada) is a patented trade name.
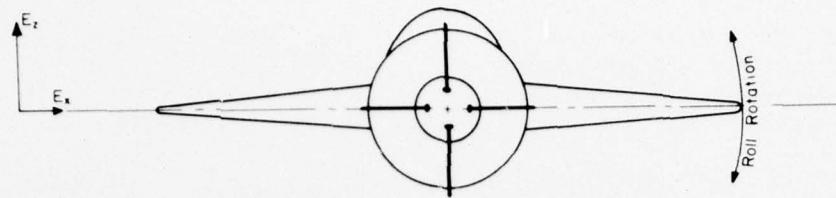
Figure 10. Front view of an aircraft system of crossed dipoles for measuring the wavetilt components E_x and E_z. The aircraft flies orthogonally to the transmitter direction.

mounted on a nose cone extending from a STOL (short take-off and landing) aircraft. The horizontal antenna is mounted orthogonally to the long axis of the nose cone. The aircraft must then fly perpendicularly to the transmitter direction for maximum coupling with E_x. This allows the more intense E_z to couple with the horizontal antenna when the aircraft rolls so that only the total E_z and the component of E_x in quadrature phase with E_z can be measured successfully to determine a wavetilt value W_q. This value is then determined along several equispaced flightpaths over the survey area.

Calibration

A wavetilt calibration is performed before and after each flight by rotating the horizontal antenna 90° to the transmitter direction for minimum coupling with E_x. This antenna is then tilted 20° to the vertical to pick up a known percentage of E_z. The E_{xq} channel is delayed 90° to read E_{xi} (in-phase component) and the signal thus recorded is proportional to $E_z \sin 20°$. The wavetilt W that this represents is

$$W = \frac{E_z \sin 20°}{E_z} = 0.34.$$

The *RF* gains of the E_{xq} and E_{zi} channels are then set to give sufficient deflection of a pen trace on an analog (chart) recorder. In-flight changes of gain in either channel are noted on the chart recorder. All data are also recorded in digital form on magnetic tape.

After a survey W_q is computed from the formula

$$W_q = \frac{0.34}{W_{cal}} \times \frac{W_{meas}}{\sin \gamma} \times \frac{A_{cal}}{A_{ope}}$$

where $W_{cal} = E_{xq\text{-}cal}/E_{z\text{-}cal}$
$W_{meas} = E_{xq\text{-}meas}/E_{z\text{-}meas}$, the ratio of the in-flight measured fields

γ = the angle between the average true azimuth of a flight line and the true azimuth from the center of the survey area to the transmitter (for maximum coupling $\gamma = 90°$)

A_{cal} = attenuator setting during calibration

A_{meas} = attenuator setting during the survey.

The strengths of the electric field quantities are recorded in volts on the magnetic tape and in millimeters on the analog chart recorder.

Flightline spacing and altitude

The choice of a flightline spacing depends on navigational, scientific and economic factors. Flightlines closer than 100 m to each other are difficult to navigate, especially over topographic relief where flight altitude must often increase. Usually the spacing is based on the field strength of a vertical dipole which, in the near field, is proportional to the reciprocal of the cube of the distance from the antenna. At an altitude of h m, the intercept of the –10 db field strength contour (relative to the ground point directly below the aircraft) with the ground is a circle of approximately $2h$ m diameter. $2h$ is then used for the flightline spacing. Over flat areas h is minimally 75 m. For particularly large surveys, the spacing must often be widened to save on expense. In this case, h is then increased to about half of the flightline spacing.

Flightpath recovery

The flightpaths are recovered with on-board photography and an altimeter. A fiducial marking system coupled to a clock drive exposes the fiducial count onto the flightpath camera film while simultaneously recording a fiducial on both the analog chart and magnetic tape. A 35-mm flight path camera, manufactured by Flight Research and equipped with a wide-angle lens, exposes a continuous film strip. The flight number and time of day are entered manually on the analog chart.

13

The aircraft height above the terrain surface is determined by a Bonzer TRN 70 radio altimeter. The output of this instrument is recorded on both the analog and digital recorders.

Data processing

The first step in the data processing is a smoothing of the vertical electric field with a 1-Hz low pass filter. Then, assuming an arbitrary wavetilt phase angle of $45°$, W is converted to apparent resistivity ρ_{qa} using eq 16.

ρ_{qa} is also filtered, again with an upper cutoff of 1 Hz. Therefore, at an average flight speed of 160 km/h, fluctuations in resistivity occurring approximately every 45 m are filtered out.

The values of ρ_{qa} and their corresponding fiducial marks are printed out in digital form. The ρ_{qa} values are then placed upon the reconstructed flight lines that are superimposed upon an aerial photomosaic reconstructed from a composite of the on-board photography. A final presentation may then be made in the form of contour maps (contouring done by hand) or as resistivity profiles along each flightline.

Ground

Technique

The commercially available Geonics EM16R* was used for the ground surveys. This instrument can measure both amplitude and phase of the surface impedance. In Figure 11 the instrument is depicted in its proper orientation for measurement with respect to the appropriate electromagnetic field quantities of a ground wave. Coil A is first used to eastablish the transmitter direction. Coil A is then shut off and the ratio of E_x, measured between two probes spread 10 m apart, and H_y, measured with coil B, is determined by adjusting the amplitude and phase dials until an inaudible null is attained. In the figure, coil A has been tilted from the horizontal to the vertical direction and is no longer coupled to H_y.

Tuning

A variety of printed circuits, each pretuned to a particular VLF frequency in present use, are available with the system. These circuits employ phase-lock amplifiers to maintain tuning.

Null detection

The achievement of a sharp null for an accurate readout depends on the signal-to-noise ratio encountered when tuning for amplitude and phase values. For
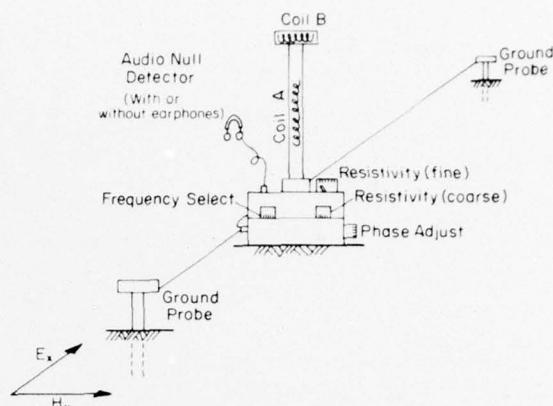
Figure 11. Schematic of the Geonics EM16R surface impedance meter. The instrument is shown in its measurement orientation with respect to the radio-wave field vectors E_x and H_y.

the sky wave mode this ratio depends on ionospheric conditions as well as the total path of propagation. For the ground wave mode, this ratio primarily depends upon distance from the transmitter. At distances within the ground wave range (≤ 800 km over earth) a readout accuracy of ±5 % for amplitude and ±0.5% for phase is usually obtained. This was true for the surveys performed in northern Maine which were slightly more than 300 km from the transmitter used.

Contact resistance

The input impedance of the ground probes is 10^8 ohms, 0.5×10^{-12} farad. Therefore, over exposed rock, a reliable measurement can be made without having the contact resistance of the probes influence the measurement. In any case, the probes need only be laid upon the ground surface.

Calibration

The EM16R is factory calibrated by applying a known voltage between the electric field probes and placing coil B within a larger coil that supplies a magnetic field of known strength. The phase discrepancy between the applied voltage and the magnetic field is adjusted and the instrument is calibrated for each of the VLF frequencies desired. The calibration considers that the hypothetical electric field is the applied voltage divided by the measurement probe spacing of 10 m.

The instrument used was bought new within one month o. ...e surveys and was calibrated prior to shipping.

14

Data reduction

The amplitude dial of the EM16R reads directly in ohm-meters of apparent resistivity. If needed, the amplitude of the surface impedance in ohms may be recovered by inverting eq 11. The resistivity scale is logarithmic and ranges from 0 to 30,000 ohm-m. The phase scale is linear and ranges between $0°$ and $90°$. This phase range is therefore based strictly on the plane-wave model described in *Principles of Electro-magnetic Resistivity Surveying* and does not allow for phase discrepancies between E_x and H_y outside of this range.

For the comparison of ground to airborne resistivity measurements, the EM16R data can be converted to an apparent resistivity ρ_{qs} based only on the quadrature value of the surface impedance and an assumed phase angle ϕ_s of $45°$. The conversion was given by eq 17.

METHODS

Experimental procedures

A topographically and geologically well-mapped site in northern Maine was selected for study. Over this site, E_z and E_{xq} of the surface mode radiation from a nearby VLF transmitter were recorded along several equispaced flightpaths at a mean altitude of 150 m. These field components were then compared using standard data processing techniques to produce an apparent resistivity contour map of the site. The map was then compared to the geology of the region.

From this standard survey, two particular flight paths were chosen and repeated at several altitudes. Along these flights both E_z and E_{xq} were measured and compared to the topography and geology below. The increase in altitude attenuated the topographic effects and allowed an examination of only the resistivity information contained in both field components. The information thus gained was later used for re-evaluating the standard survey with topographic effects removed.

Part of the standard survey was then repeated at twice its mean altitude to study the effect of altitude upon two-dimensional geologic resolution and mean apparent resistivity levels. This repeated survey used a lesser flightline spacing than the standard survey. Therefore, a few additional flightlines were added to the standard survey so that both surveys had an equal number of flightlines over the same area.

An extensive ground survey of Z_s determined the individual effects of phase and amplitude upon the standard survey results. Traverses were made over all major rock types present. In a few cases, the ground readings obtained were used to verify the topographic corrections applied to the airborne readings.

In Table I is presented a summary of the specifications for all the airborne and ground studies.

Table I. Study specifications.

Study no.	Description and purpose	Mean flight altitude (m)	No. of flights	Mean flightpath length (km)	Mean flight spacing (km)
1	Low altitude standard survey — geologic delineations using standard techniques.	150	13	10	0.4
2	High altitude series A — topographic and resistive effects upon E_z and E_{xq} of study 1.	90	1	10	
		150*	1	10	
		300†	1	10	
		600	1	10	
	High altitudes series B — same purpose as series A.	90	1	10	
		150*	1	10	
		300†	1	10	
		600	1	10	
3	Low and high altitude surveys — altitude effects on geologic delineations of study 1.	150**	10	10	0.16
		300	10	10	0.16
4	Ground survey — amplitude and phase effects upon geologic delineations of study 1.	0			

* Adapted from study 1.
† Adapted from study 3.
** Includes 6 flightlines of study 1.

15
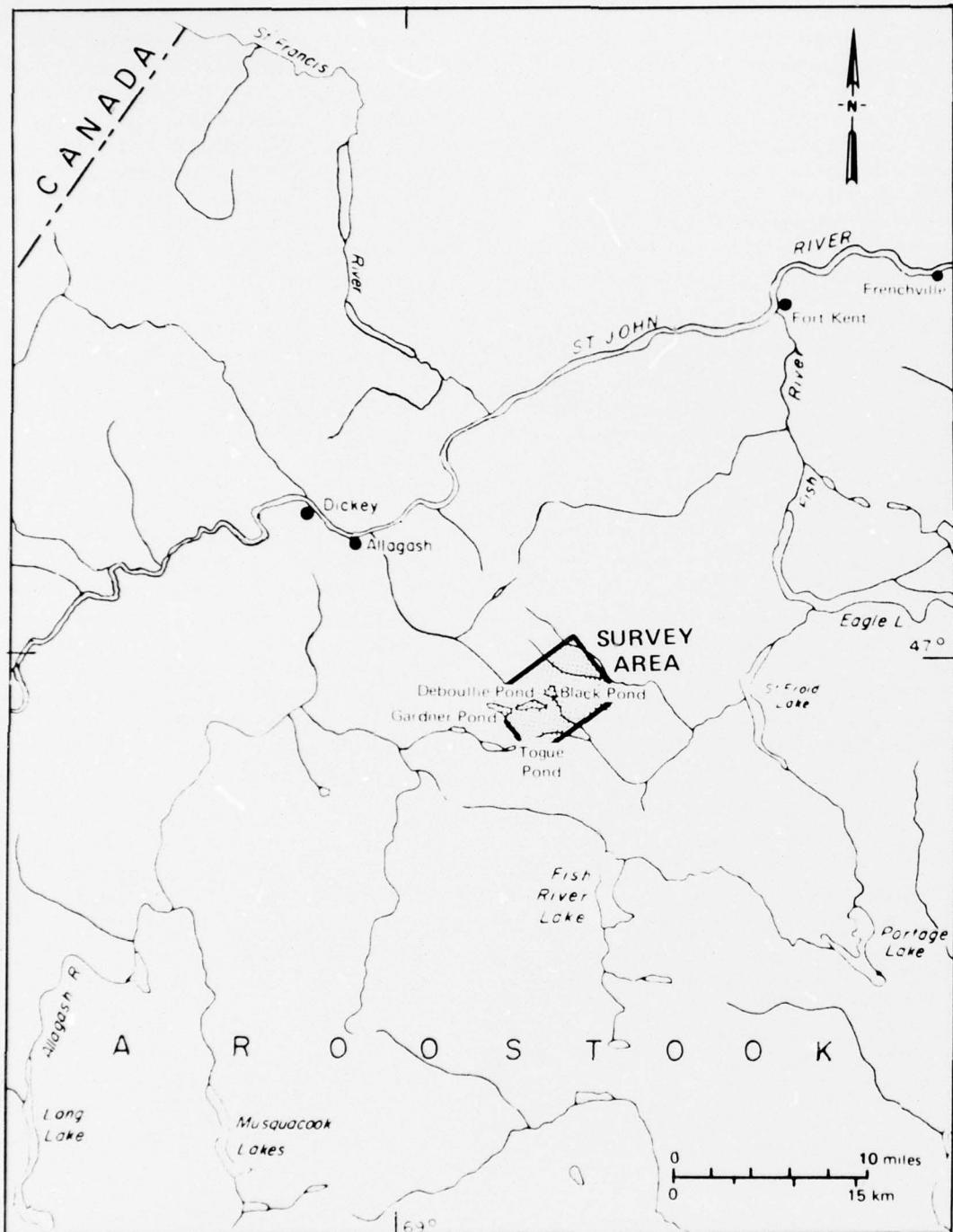
Figure 12. Location of the survey area in northern Aroostook County, Maine.
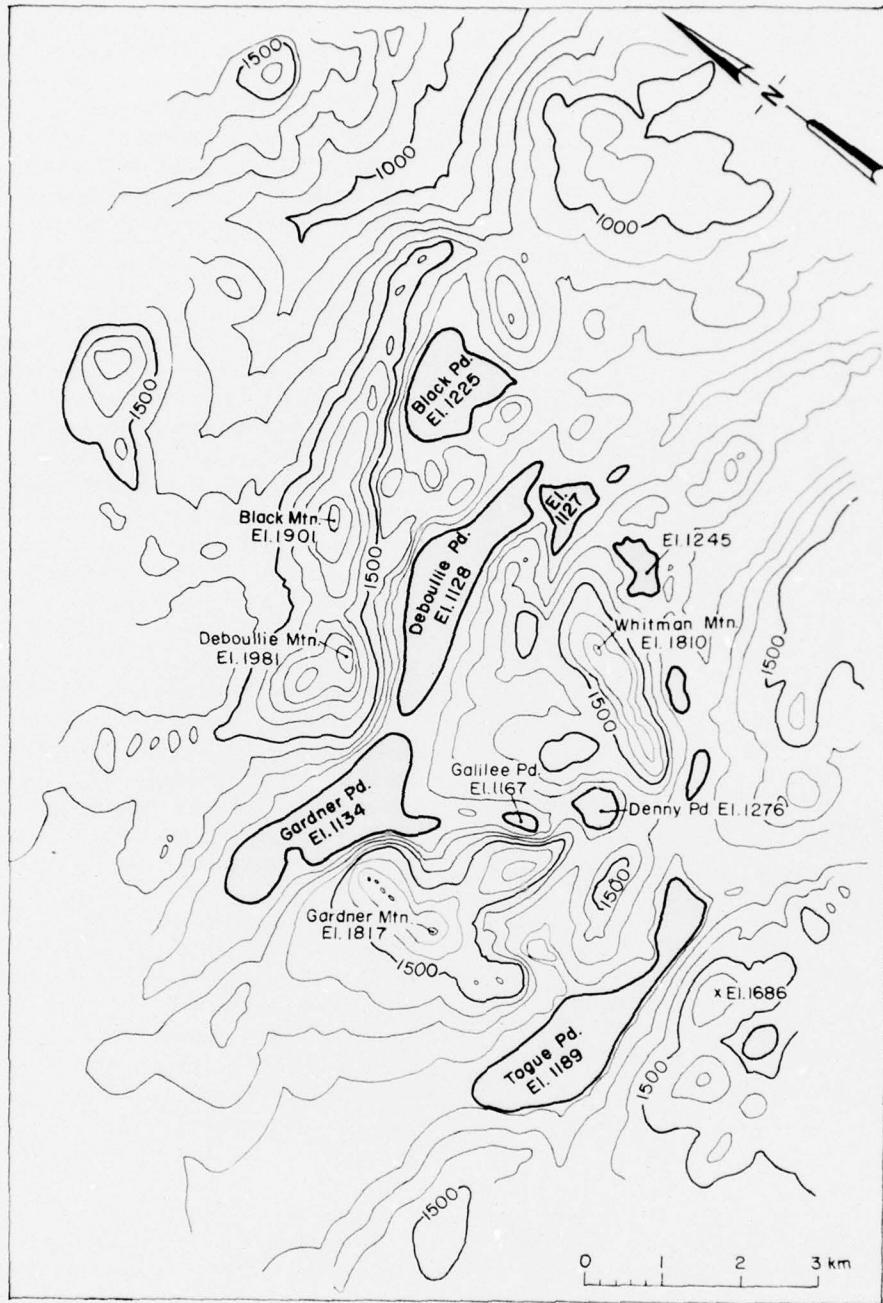
Figure 13. Topographic contours and elevations of the survey area. Elevations are in feet.

Test site

Location

The area chosen for the experimental survey (see cover photograph) is shown on the map in Figure 12. It is located approximately 19 km southeast of the confluence of the St. John and Allagash rivers in the Deboullie Mountain area and is currently a state park. The area is accessible only by numerous logging roads which are passable by truck between about 1 June and 1 November. In nearby Frenchville, Maine, there is an airport which was used for the mobilization of the flight crew.

17

Figure 14. Geology of the survey area (after Boone 1962).

The relief is often severe with many elevations falling off quite rapidly. From Deboullie Peak to the shore of Deboullie Pond, the elevation decreases by 800 ft (240 m) over a horizontal distance of approximately 1600 ft (480 m) and parts of this flank are rock slides. Along other flanks, as at the southwest shore of Galilee Pond, these falloffs are actually sheer cliffs.

Geology

The bedrock geology of the test site, an igneous stock surrounded by slate (designated Seboomook* slate), is shown in Figure 14 (after Boone 1962). The intrusive stock is divided into a northern section of predominantly syenite and a southern section of granodiorite. There are a few smaller inclusions of slate in the syenite. The southerly slopes of Deboullie and Black mountains are syenite while the northerly slopes are slate. The western slope of Gardner Mountain is slate while the eastern half is syenite and granodiorite. The western slope of Whitman Mountain is granodiorite while the eastern slope is slate. The dip of the slaty cleavage is commonly greater than 70° and the strike is northeast to southwest. Geologic profiles at depth have not been made.

The surficial geology of the region is generally a glacial till (McKim and Merry 1975) of less than 1.0 m thickness. The lower elevations, where sediment accumulation would be expected to be greatest, are dominated by the pond chains.

VLF electromagnetic characteristics

Station NAA (17.8 kHz) located 300 km to the southeast near Cutler, Maine, was monitored for all surveys. The transmitter is a top-loaded vertical electric monopole with an effective radiation of 890 kW of continuous power. This transmitter, as are most other VLF transmitters, is in regular use by the United States Navy for submarine communication. Information is transmitted by amplitude modulation allowing the phase lock circuitry of the receiving equipment used in the experiments to stay tuned.

NAA's distance falls within the limit (307 km at 17.8 kHz) defined by eq 1 and thus allows an evaluation of the relative contributions of both the surface and sky modes to the total vertical electric field strength. This calculation is important because it demonstrates that the VLF signals received were not subject to ionospheric conditions. From eq 2 and 3, the formulas for the relative contributions of both surface and sky modes in decibels above 1 μV/m as derived in Watt (1967) are

---

* Early Devonian Age — Seboomook is a regional designation.

Topography

The test site is situated in a small mountainous belt that continues in a north-south direction and lies at a mean elevation between 1000 and 1500 ft (300-450 m). The topographic contours, simplified from the U.S. Geological Survey topographic map for the Fish River Lake quadrangle, are shown in Figure 13. The area contains several large ponds which dominate the low elevations. The high elevations are dominated by Gardner, Whitman, Deboullie, and Black mountains, all of which rise between 700 and 800 ft (210-240 m) above the ponds.

$$E_{z_{\text{surface}}} \,[\text{db}, 1\,\mu\text{V/m}] = 109.5 + 10 \log P_r$$

$$- 20 \log d + 20 \log |F| \quad (21)$$

$$E_{z_{\text{sky}}} \,[\text{db}, 1\,\mu\text{V/m}] = 103.5 + 10 \log P_r$$

$$- 20 \log (d + \Delta d) + 10 \log G_t \,(\alpha, \psi)$$

$$+ 20 \log F_t + 20 \log |R_m| + C_m$$

$$+ 20 \log F_r + 20 \log (\cos \psi) \quad (22)$$

where d and P_r are expressed in kilometers and kilowatts, respectively.

These formulas are for ground-based transmitting and receiving antennas.

Considering only a one hop sky mode transmission, an ionospheric height of 75 km, an ionospheric resistivity of 10^5 ohm-m,* and a maximum average ground resistivity of 500 ohm-m, the terms in these equations evaluate as follows:

$$P_r = 890 \text{ kW}$$
$$F = 1.0$$
$$\Delta d = 36 \text{ km}$$
$$\alpha = 63°$$
$$\psi = 27°$$
$$G_t = 0.79$$
$$F_t = 2$$
$$F_r = 2$$
$$20 \log |R_m| = -32 \text{ db}$$
$$C_m = 0.4 \text{ db}.$$

Substituting these values into eq 21 and 22, the relative vertical electric field strengths at a distance of 300 km from station NAA are

$$E_{z_{\text{surface}}} = 89.5 \text{ db}, 1\,\mu\text{V/m}.$$

$$E_{z_{\text{sky}}} = 59.5 \text{ db}, 1\,\mu\text{V/m}.$$

Since E_z has been measured at well above 66 db above $1\,\mu\text{V/m}$ (U.S. Naval Research Laboratory, signal level contours, station NAA), these calculations ensured that only the surface wave mode was present and that interference between the two modes and ionospheric effects would not be of any significance.

In Table II is presented a summary of previous VLF investigations in the area (after Sellmann et al. 1975) taken at 17.8 kHz.

Since these phase angles are considerably below 45°, it was expected that both phase and amplitude would play a significant part in the results of an airborne survey.

Survey traverses

Study no. 1 – standard survey

The flightlines of this survey are shown superimposed on the topography in Figure 15. A mean altitude of 150 m was prescribed for the entire survey; at this altitude 300 m is about the optimum flightline separation. However, the altimetry of Hoekstra's surveys (Hoekstra et al. 1974) had revealed that pilots tend to fly too high when encountering steep relief. Therefore, the spacing was prescribed at 400 m which then required 13 flightlines to cover the area.

Table II. Summary of previous investigations at 17.8 kHz in the vicinity of Deboullie Mountain, Maine (after Sellmann et al. 1975).

Rock type	Location	No. of measurements	ρ_a (10^3 ohm-m)	ϕ (degrees)
Syenite	Deboullie Mtn.	3	9-30	13-23
Granodiorite	Gardner Mtn.	10	12-30	15-40
	Whitman Mtn.	14	3.8-27	22-35
Slate	Togue Pond	3	10-11	22-29

* This is based on the average values of 1.4×10^6 Hz for ion collision frequency and $5 \times 10^8/\text{m}^3$ for electron density (Watt 1967).
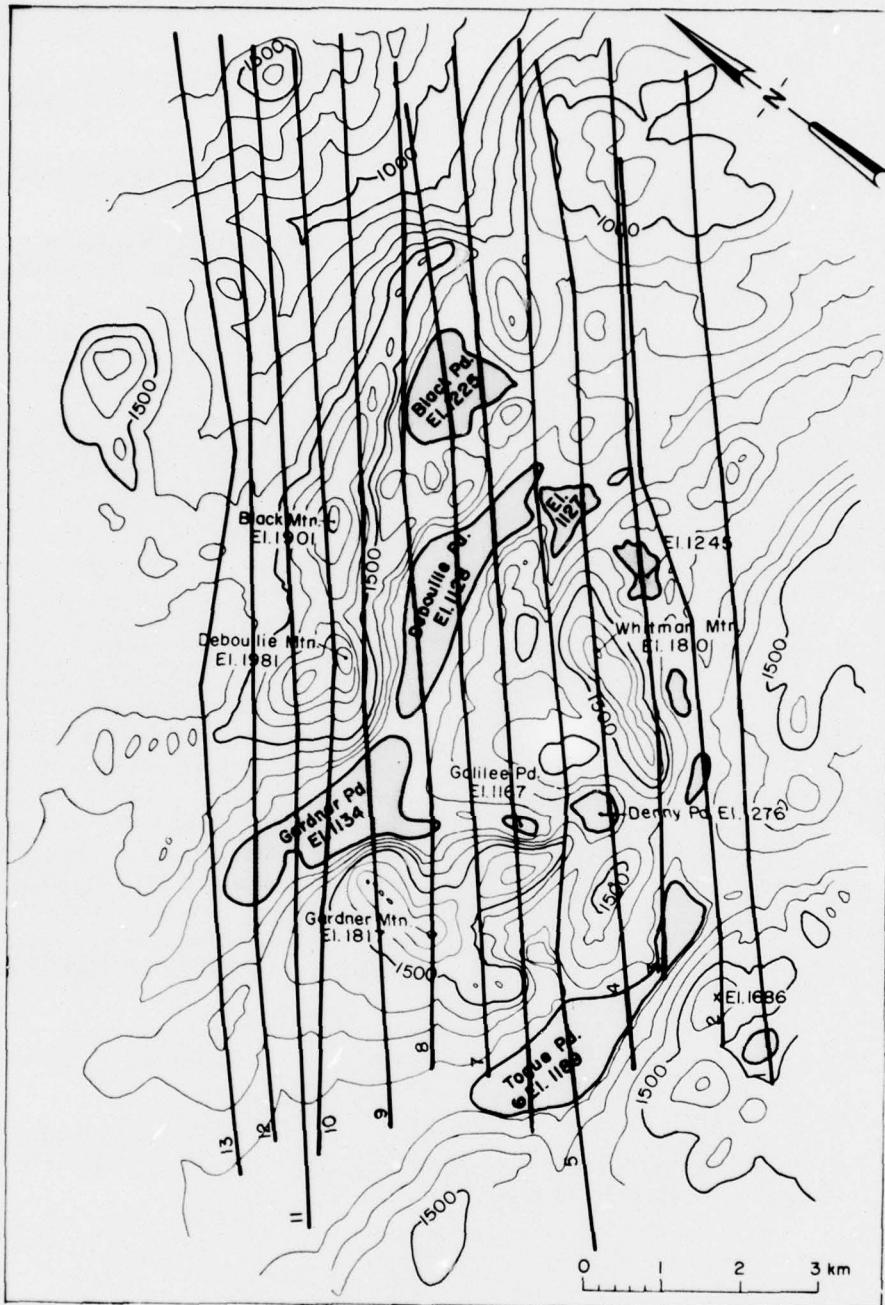
Figure 15. Flightpaths of the standard survey conducted at a mean altitude of 150 meters.

As shown in Figure 15, the flightlines covered all the major rock types, topographic features and major ponds. The slight changes in flight direction were caused by attempts to navigate equispaced flight-paths (the pilot fixed on predetermined landmarks). The mean azimuth bearing of the flightlines γ with respect to the trans- mitter direction was 81°. As the Deboullie Mountain area is wilderness, no interference from any power or telephone lines or any other man-made structures was possible. This and the following airborne surveys were conducted between 22 September and 5 October 1975.

20

Flight Altitude

——— 90 m
········ 150 m
—·—·—300 m
————600 m
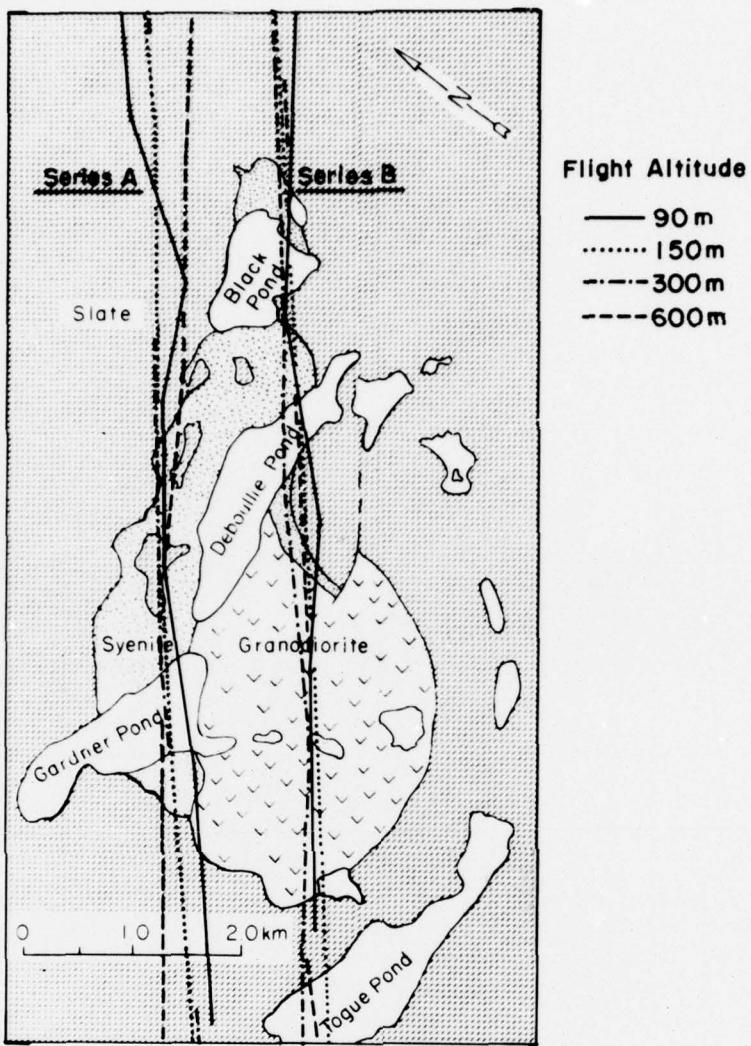
Figure 16. Flightpaths of high altitude series A and B.

Study no. 2 – high altitude series

Flightpaths 6 and 9 of Figure 15 were repeated because of their horizontal position over Gardner, Deboullie and Black mountains and because they traversed the slate, granodiorite, syenite and the ponds. Three additional altitudes were added to each of these flightpaths and are shown superimposed upon the geology in Figure 16. The mean altitudes flown were 90, 150 (of the standard survey), 300 and 600 m, as indicated. It was expected beforehand that by 600 m all topographic influence upon the VLF fields would disappear in accordance with the observations of Harrison et al. (1971) discussed previously. The two separate flight groups are distinguished as series A and series B.

Study no. 3 – high and low altitude standard surveys

A more intensive survey of 160-m mean flightline spacing and 300-m mean altitude over the central section of the test site was chosen for this study. The central portion chosen was suspected to be well within a high resistivity zone so that the lower resistivity zones that may have existed to the northwest and southeast of the survey limits would not affect the 300-m survey any more than they would the 150-m survey. Four flightlines were then added between flightlines 5 and 10 of the 150-m standard survey to allow comparison. The flightlines of both these surveys are shown in Figure 17 superimposed over the geology. The figure reveals how difficult it was to

21

a. 150 m.   b. 300 m.
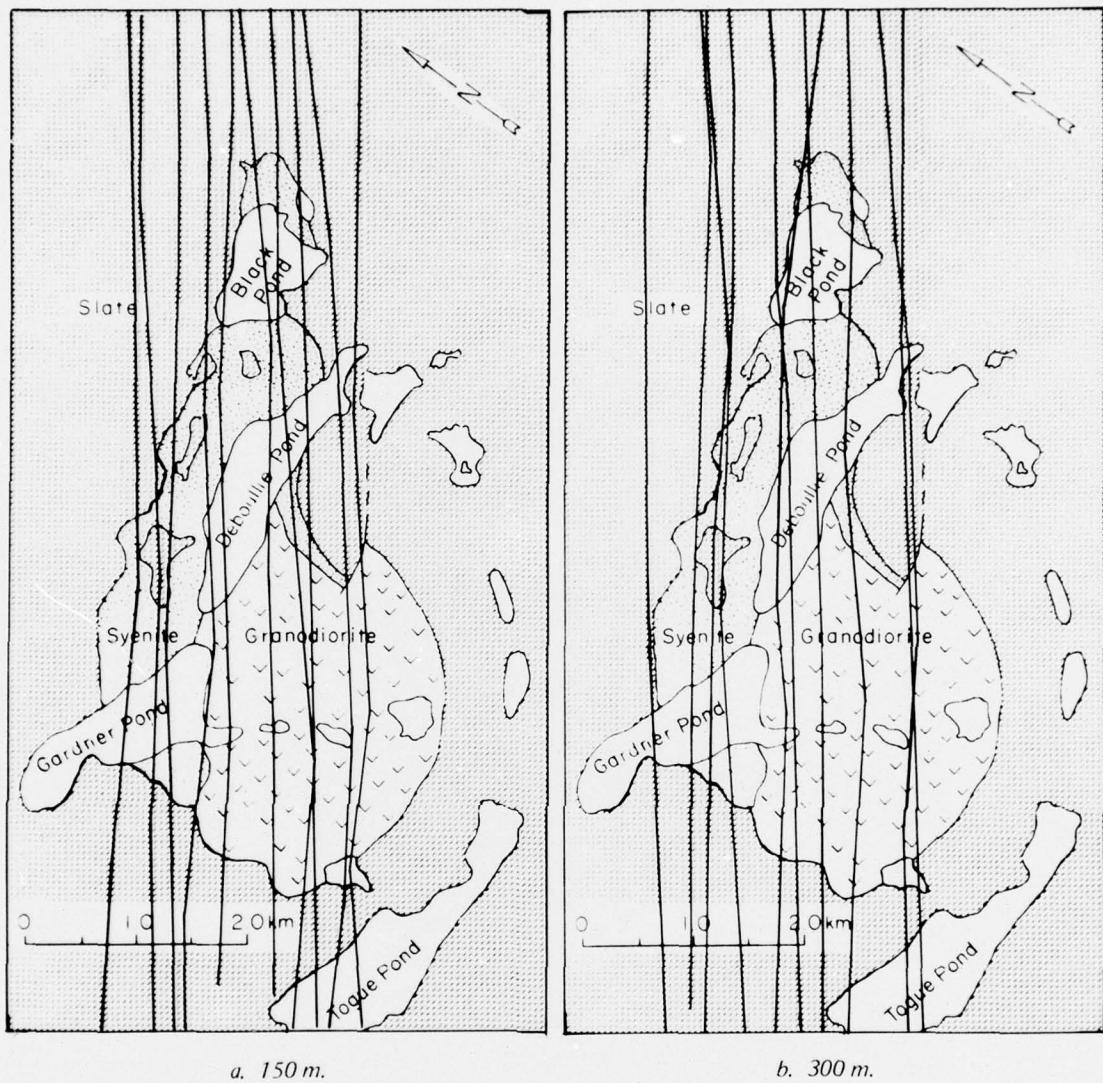
Figure 17. Flightpaths of the (a) low and (b) high altitude standard surveys.

navigate equispaced flightlines. Therefore, it must be emphasized that the prescribed line spacings are mean values.

Study no. 4 – ground surveys

The ground traverses made in relation to the topography of the area are shown in Figure 18 accompanied by a legend of the rock types encountered. Measurements of the surface impedance phase and amplitude were made every 60 m. At a few measurement stations the electric field probes of the Geonics EM16R were rotated 90° to find if the tangential electric field

deviated from the transmitter direction. The results were always negative. The word "tangential" is used rather than horizontal because rarely were the electric field probes exactly on a horizontal plane. Usually they were tilted a few degrees to the vertical, since many measurements were made along flanks that dipped down from the transmitter direction. The apparent resistivity and phases over the ponds are inferred from previous measurements over New England ponds where ice makes them accessible in the winter (Parrot and Fleming 1970).
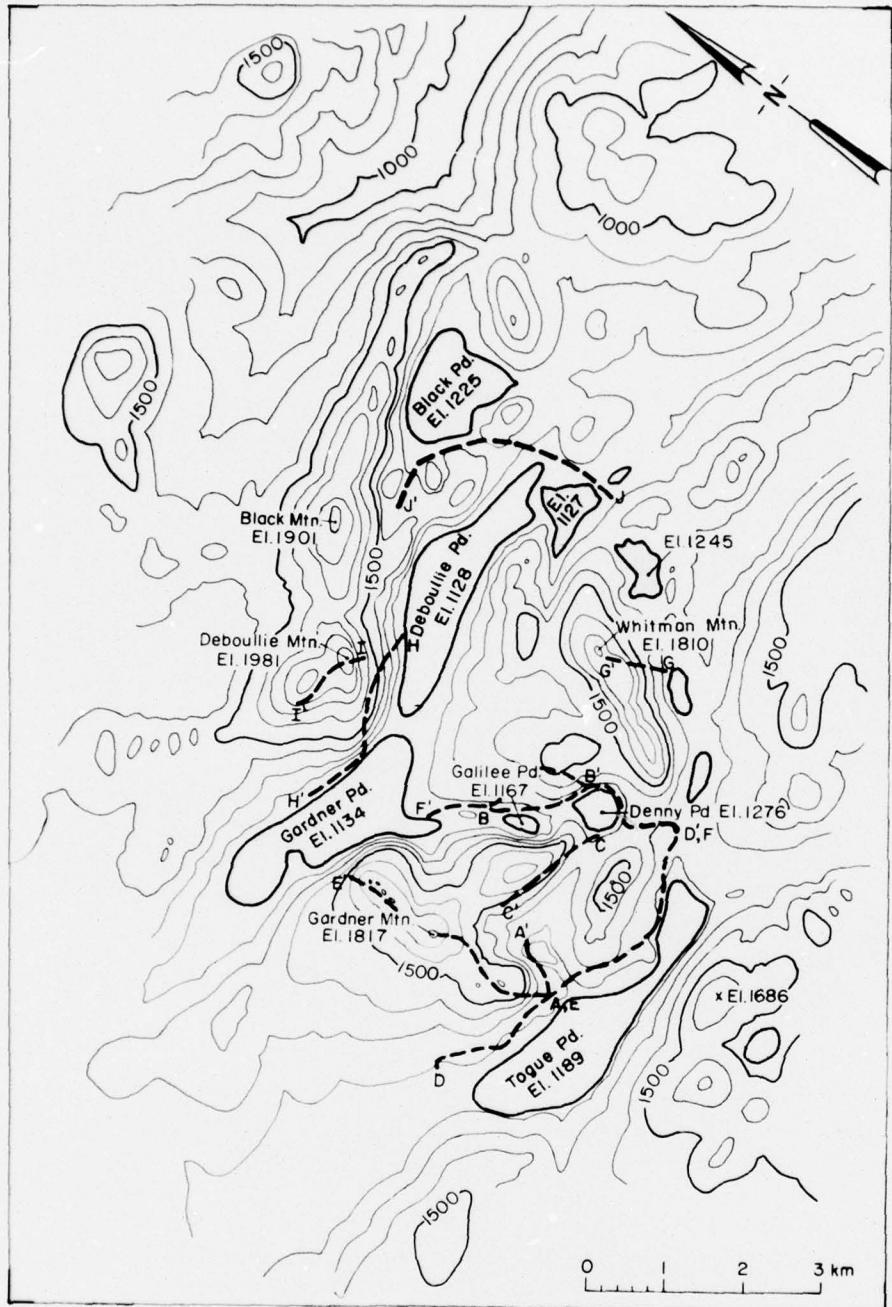
22

Figure 18. Ground traverses made over the survey area. Unprimed letters denote the start and primed letters denote the finish of the traverse. Rock types are given in the sequence in which they were encountered. Elevation contours are in feet.
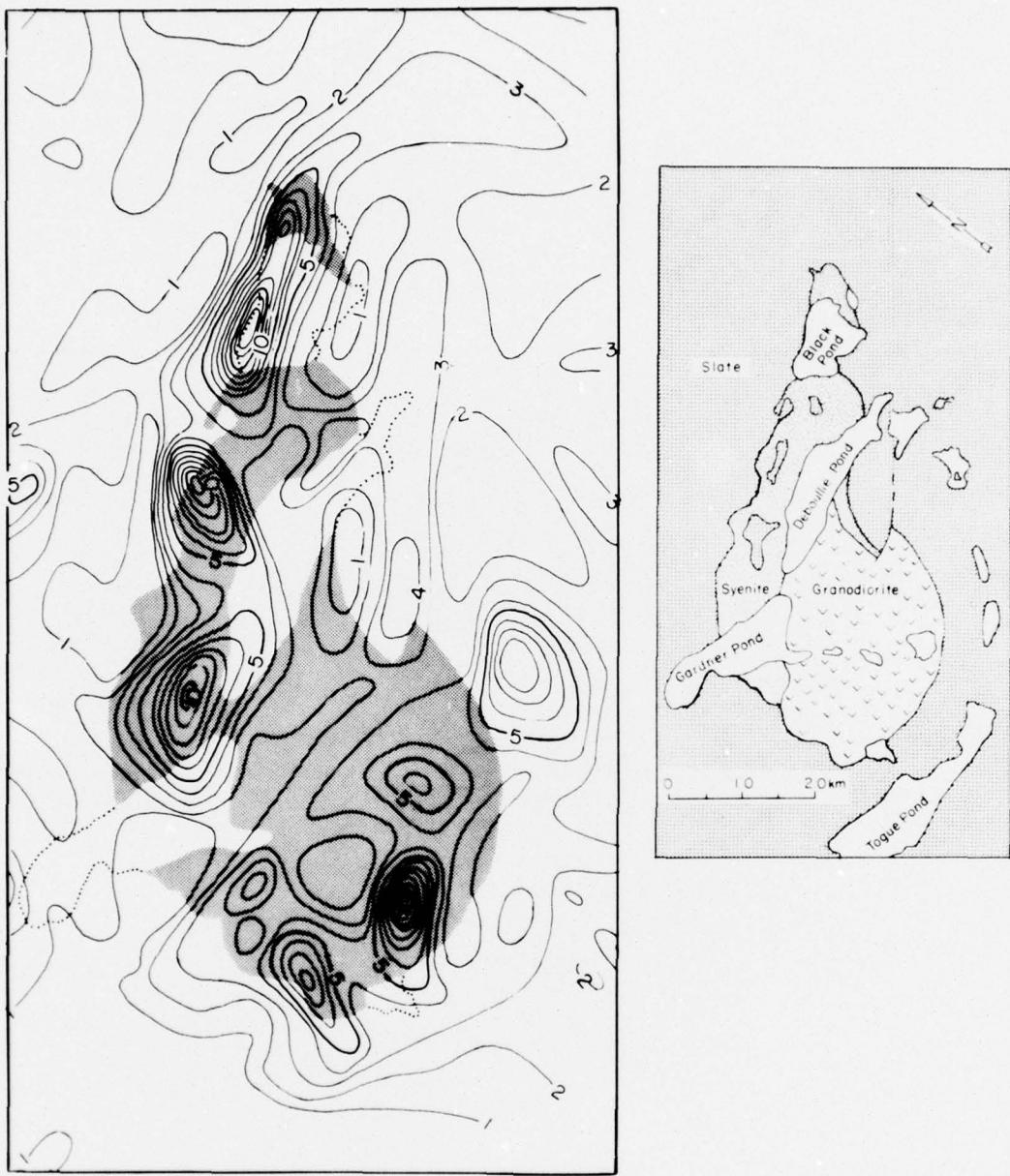
Figure 19. Apparent resistivity ρ_{qa} contours superimposed upon the geology. Shaded areas are syenite and granodiorite. Contour values are given in thousands of ohm-meters; mean flight altitude is 150 m.

RESULTS

Study no. 1 – standard survey

The results of the standard survey are presented in Figures 19, 20 and 21. Figures 19 and 20 show the resistivity patterns superimposed on the geologic and topographic bases. These patterns were hand contoured from the digitized resistivity values computed along each flightline. The contours are given in 1000 ohm-m intervals. Also shown in Figure 19 is the geologic base by itself to facilitate the comparison.

The most important features of Figure 19 are the more intense, higher resistivity anomalies that are mostly associated with the granodiorite and syenite. Over the granodiorite there are anomalies of 5000, 6000, 8000 and 12,000 ohm-m. Over the syenite there

24
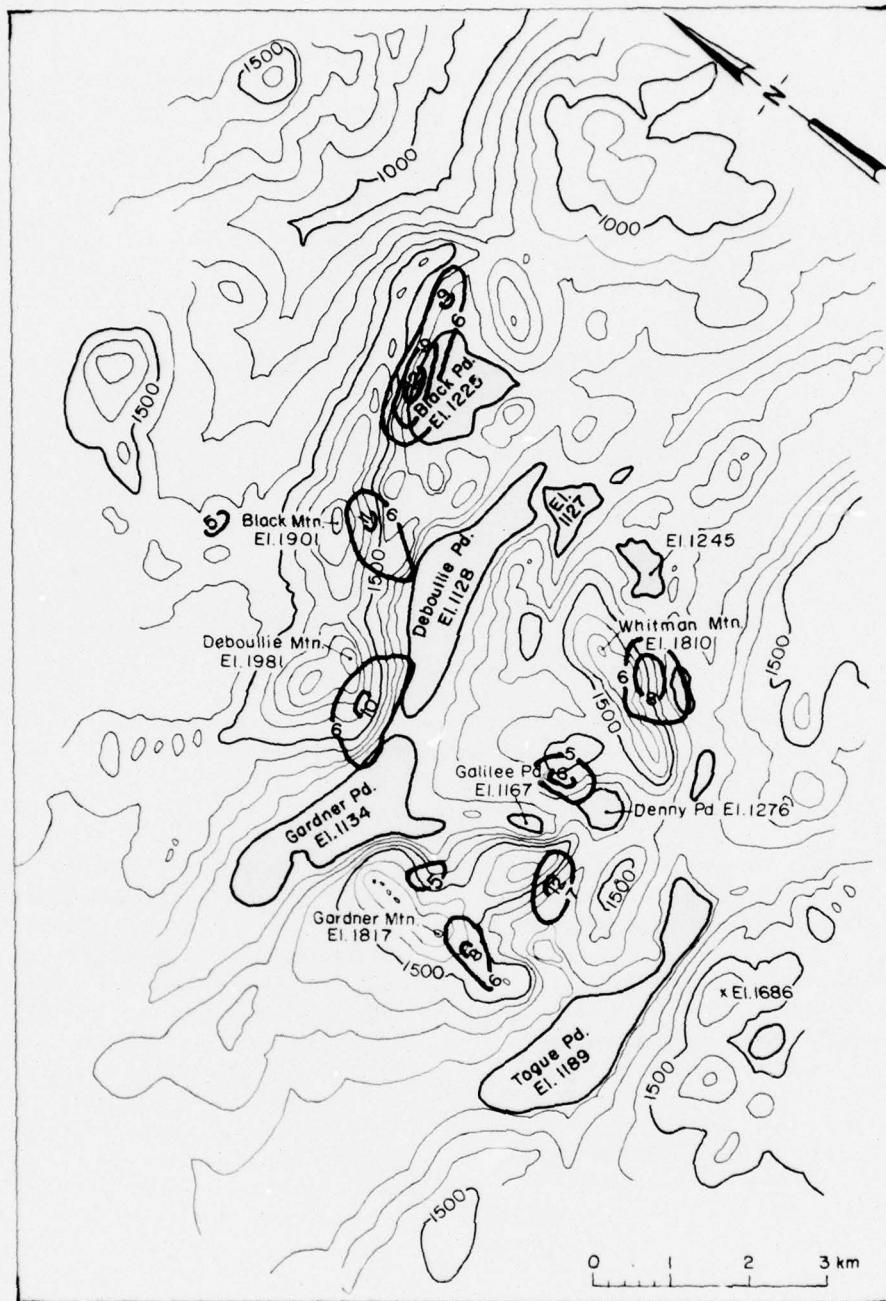
Figure 20. Anomalous high resistivity zones superimposed upon the topography. Resistivity contour values are given in thousands of ohm-meters; elevation contours are in feet.

are anomalies of 9000, 10,000 and 11,000 ohm-m. The slate, which occupies the largest area of the survey, is generally dominated by the 2000 and 3000 ohm-m contours, but there are three anomalies of 5000 ohm-m (just above left center), 8000 ohm-m (just below right center — actual value is 8900) and 12,000 ohm-m (just north of Black Pond). The pond areas contain no high anomalies, as should be expected, but they are obviously influenced by the large anomalies that border their shores. Lake water usually has resistivity values

25
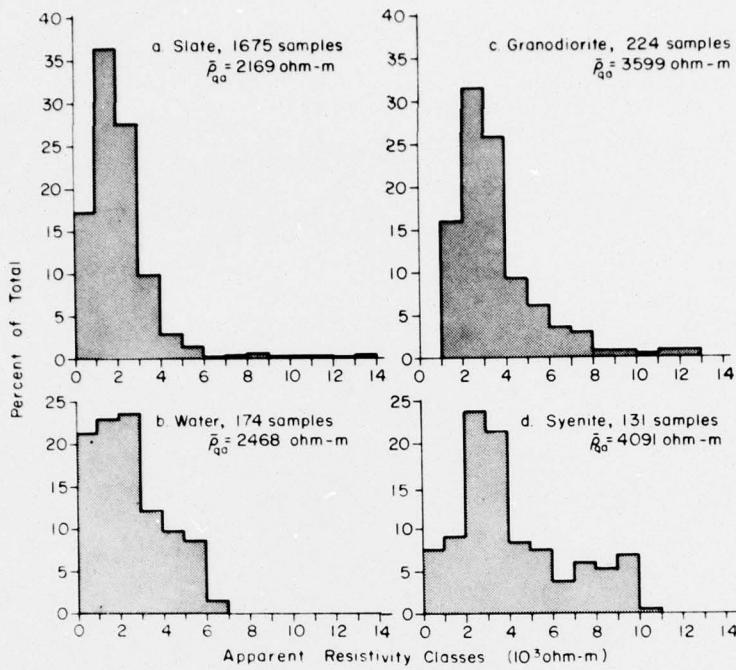
Figure 21. Normalized distributions and means of the digitized standard airborne resistivity values ρ_{qa} for the four major materials of the survey area. Flight altitude is 150 m.

of less than 200 ohm-m. However, the larger ponds very gradually deepen to more than 20 m so that values near 1000 or 2000 ohm-m are not unreasonable near the shores.

The location of the high resistivity anomalies in relation to the topography is shown in Figure 20. Without exception, the points of highest resistivity fall on mountain flanks (note that the aircraft did not avoid the peaks — see flightpaths shown in Figure 15). The reason is that the lower elevations are dominated by the lower resistivity pond chains, while over the higher elevations (ridges) the reference field E_z was enhanced, as will be shown in the next section. It should also be noticed that there are many flanks located over all rock types, especially in the igneous zone south of Gardner and Deboullie ponds and just west of Black Pond, which are not unusually high resistivity areas. Above about 6000 ohm-m there is a definite differentiation among mountain flanks, even within one rock type, and a definite discrimination against mountain ridges. Therefore, the actual coverage of, say, the igneous geology could not be correctly inferred from Figure 20.

Figure 21 gives the normalized distributions and means of the digitized resistivity values for each of the four major material types of the area. The rock ranges generally fall within the broad range specified for crystalline rock in Figure 2. As expected from the contours, the slate is measured as the least resistive rock, with 64% of all values falling between 1000 and 3000 ohm-m and a mean value of 2169 ohm-m. The syenite is measured as most resistive, giving the highest average and the heaviest distribution between 5000 and 10,000 ohm-m. The fact that most of the higher airborne resistivities are associated with the intrusive geology seems to indicate that the intrusives are far more resistive than the slate. On the contrary, it will be shown that the slate is actually of comparable resistivity and that the hidden factors of topography and wavetilt phase often determine whether a topographic or geologic area is mapped as an airborne anomaly or not.

In the following sections, the separate influences of topography, altitude and the amplitude and phase of the wavetilt upon this survey are experimentally analyzed.

Study no. 2 – topographic and resistive effects upon E_{xq} and E_{zi}

In this study, topographic effects upon E_{xq} and E_{zi}
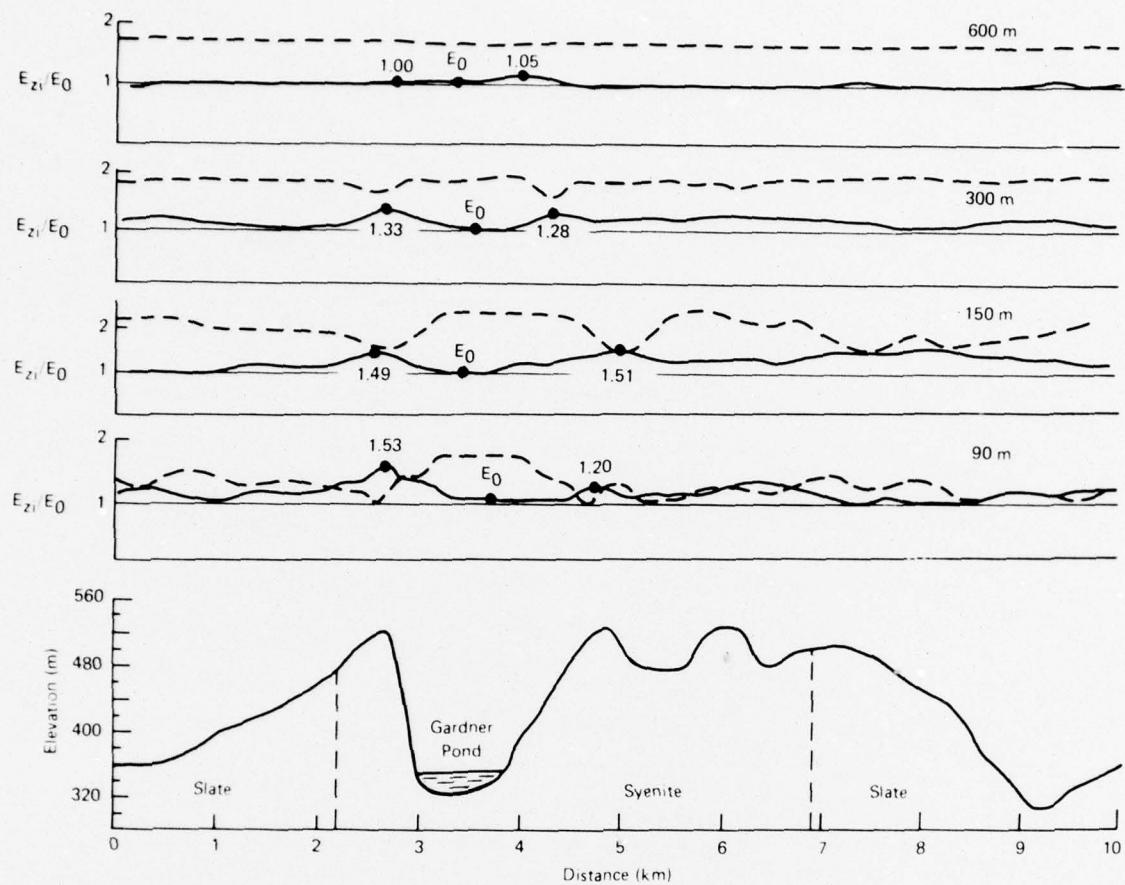
Figure 22. Uncalibrated altimetry (broken) and normalized E_{zi} (solid) analog traces along the flightpaths of altitude series A. The traces are not exactly coincidental with each other or with the topographic profile because of changes in flight speed. Note that in the 90-m trace E_{zi} tends to return to nearly the same level during periods of stable altimetry irrespective of the geology and that at 600 m the disturbances have nearly disappeared.

are separated from resistivity effects when the altitude of two particular flightpaths is increased to values comparable (300 m) and above (600 m) the mountainous relief itself. It is assumed that any topographic effects upon E_{xq} are attenuated with altitude as rapidly as those upon E_{zi}, allowing only the resistivity responses of the two field components to remain at the higher altitudes. The traces of the individual field components are not calibrated in terms of absolute field strength because transmitter power and gain levels varied over the several days that the flights were carried out.

Figures 22-25 show the normalized analog traces of E_{zi} and E_{xq} and the uncalibrated altimetry for the flightpaths in Figure 16. The topographic and geologic cross sections are shown at the bottom of the figures. The altimeter traces are uncalibrated but terrain clearance increases upwards. The altitude levels given are

approximate mean values. The different profiles within a particular series are not all exactly coincidental with each other or with the topographic profile because of changes in flight speed that resulted from whether a flight was from southwest to northeast or vice-versa. Therefore, for each trace the altimetry must be used to recognize where a particular disturbance takes place. In all figures the topographic vertical scale has been magnified by a factor slightly greater than 10.

Figures 22 (series A) and 23 (series B) show the traces of E_{zi}. The normalization values E_0 correspond to the more stable altimetry over Gardner and Togue ponds (Fig. 22 and 23). At 90-m and 150-m mean altitudes E_{zi} increases above all the higher land elevations (this is seen more clearly by the coincidence of the altimetry changes with the E_{zi} changes), in these cases very near the mountain peaks. Since ρ_{qa} is inversely proportional to the square of E_{zi}, these

27
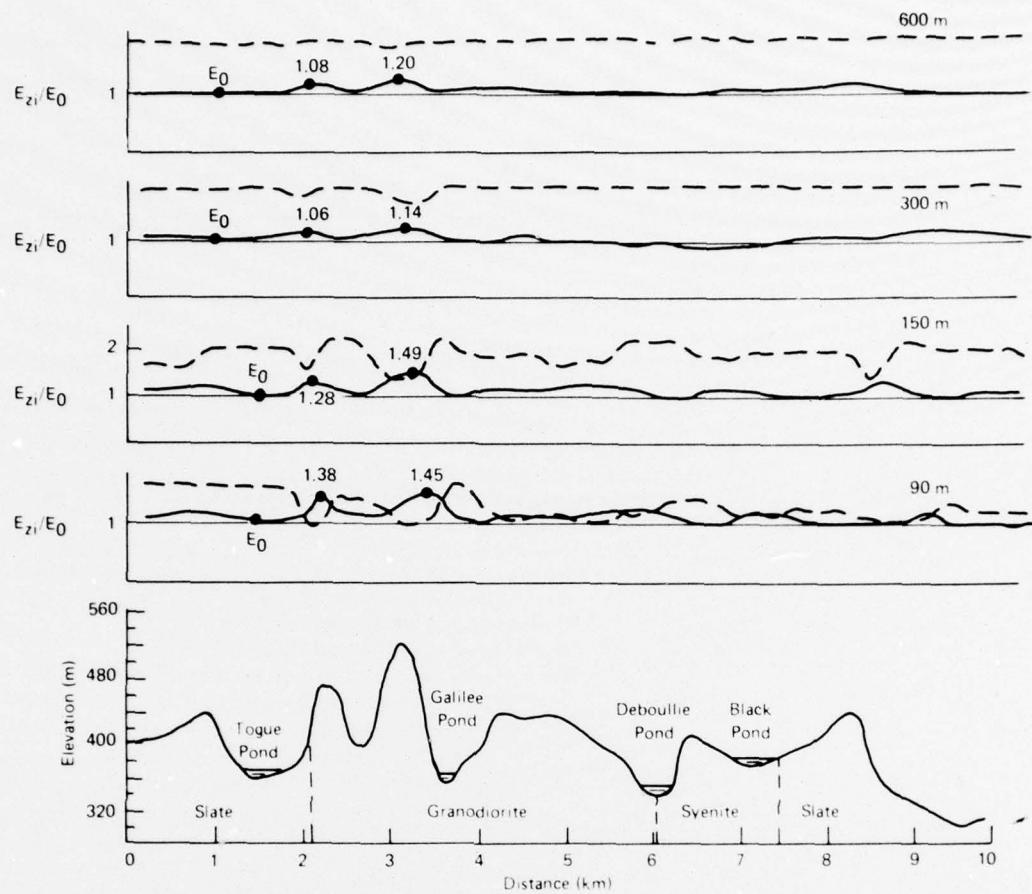
Figure 23. Uncalibrated altimetry (broken) and normalized E_{zi} (solid) analog traces along the flight-paths of altitude series B. The traces are not exactly coincidental with each other or with the topographic profile because of changes in flight speed. Note that in the 90-m trace E_{zi} tends to return to nearly the same level during periods of stable altimetry, irrespective of the geology.

traces now reveal why the anomalies of Figure 20 were confined to the mountain flanks. At the 300-m level the fluctuations have become much less intense and they have practically disappeared at the 600-m level of series A. It should also be noticed that along the 90-m traces, E_{zi} always tends to return to nearly the same level over the flatter portions of the topographic profile, irrespective of the geology.

These observations of E_{zi} are similar to those of Harrison et al. (1971) as mentioned above, but for this study they define the 600-m altitude level as the approximate limit of topographic or resistive influence upon E_{zi} and, therefore, the assumed limit of topographic influence (if any) upon E_{xq}. In the E_{xq} traces of Figures 24 (series A) and 25 (series B), the normalization values were again taken above Gardner (Fig. 24) and Togue (Fig. 25) ponds. As with the E_{zi} traces, all the perturbations have attenuated with height. How-

ever, at 600 m large resistivity perturbations still remain. They are much larger than the perturbations in the 600-m E_{zi} traces, especially those of Figure 22 where there are only negligible changes above the same topographic features.

Since all the above field strength traces are uncalibrated in terms of amplifier gain, the effect of resistivity upon only E_{xq} at an altitude above topographic influence is best illustrated in the apparent resistivity profiles (solid curves) of Figures 26 (series A) and 27 (series B) because they account for the calibration of both field levels. At the 600-m altitude of both flight series the resistivity values may be seen to vary between 1000 and 7000 ohm-m for series A and between 1700 and 5000 ohm-m for series B. Since ρ_{qa} is proportional to $(E_{xq}/E_{zi})^2$, E_{xq} varies by as much as a factor of 2.78 as compared to 1.05 for E_{zi} at 600 m for series A. For series B E_{xq} varies by as much as a

28
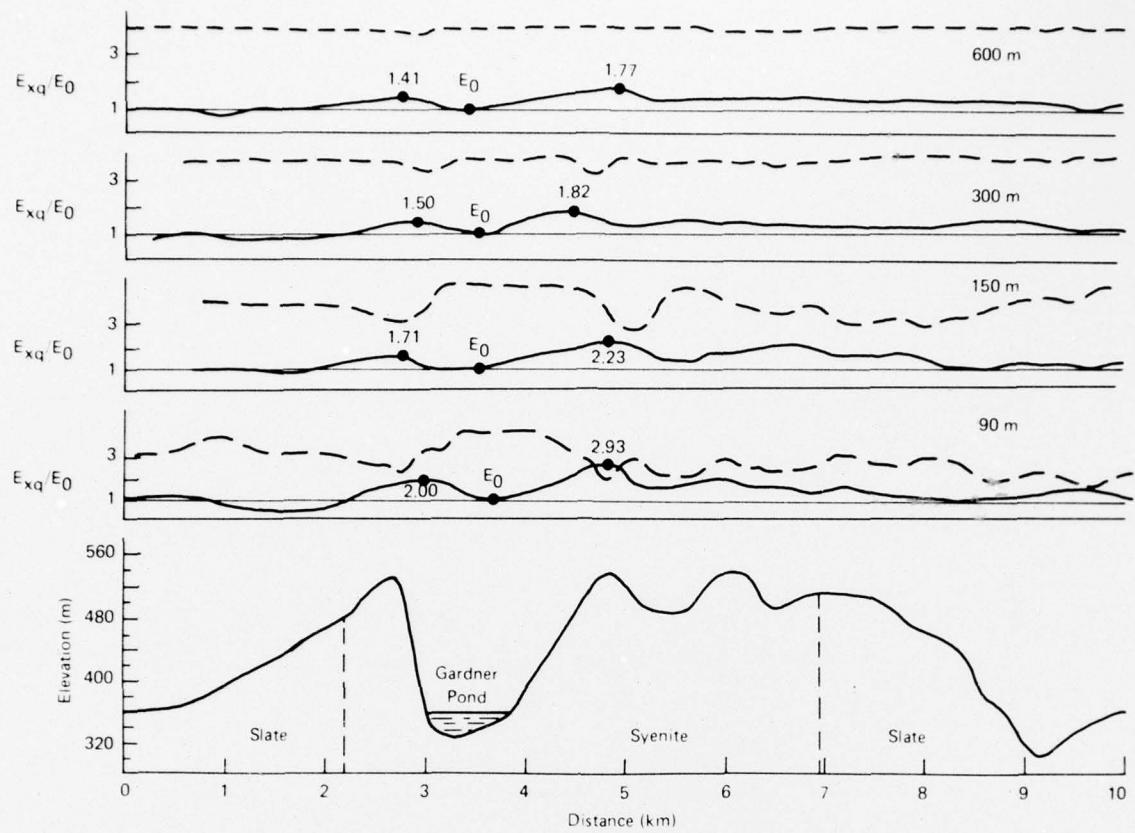
Figure 24. Uncalibrated altimetry (broken) and normalized E_{xq} (solid) analog traces along the flightpaths of altitude series A. Note that at 600-m mean flight altitude the fluctuations in E_{xq} are much more intense than they were in Figure 22 for E_{zi} over the same topographic features.

factor of 2.06 compared to 1.20 for E_{zi}. It therefore seems evident that when topographic effects are eliminated only E_{xq} is essentially responsive to resistivity changes.

It may be noticed in these figures that the lower altitude (90- and 150-m) profiles are not entirely consistent with the high altitude (300 and 600 m) profiles. In Figure 26 the Gardner Mountain anomaly is too low at 90 and 150 m, and at 150 m the Black Mountain anomaly is relatively too high compared with the same anomaly in the other three profiles. In Figure 27 the mean values at 90 and 150 m are inconsistently low, since they are so much closer to the igneous area. However, a significant improvement results when the resistivities are recomputed (dashed curves) using only the reference area levels E_0 of Figures 22 and 23 for E_{zi}. Now the syenite anomalies at 90 and 150 m over Gardner Mountain in Figure 26 are more consistent with those at the higher altitudes, with each other, and

also with the other syenite anomalies over Deboullie and Black mountains. The Deboullie Mountain anomaly at 150 m is now the largest at this altitude as it is at all other altitudes. In Figure 27 the mean values for the different altitudes are all now more comparable and the anomalies to the right of Galilee and Deboullie ponds have been enhanced at the 90-m level to their corrected values at the 150-m level. For both series the 300-m and 600-m profiles have changed marginally as is to be expected.

Study no. 3 – general effects of altitude upon geologic resolution

The altimeter traces of Figures 22-25 revealed that it was very difficult to maintain constant terrain clearance, although the flight altitude relative to sea level was probably much more constant. The kind of relief encountered can present a serious danger to an aircraft trying to maintain a low survey altitude and the variability in

29
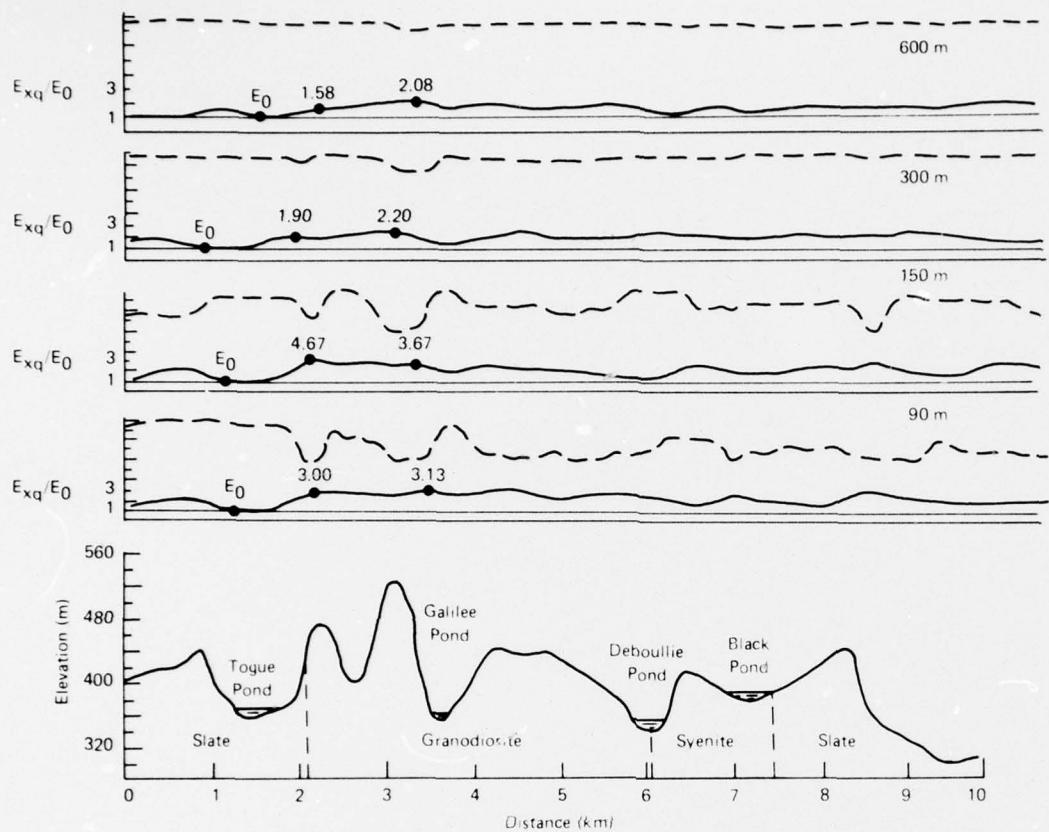
Figure 25. Uncalibrated altimetry (broken) and normalized E_{xq} (solid) analog traces along the flight-paths of altitude series B. Note that at 600-m mean flight altitude the fluctuations in E_{xq} are much more intense than they were in Figure 23 for E_{zi} over the same topographic features.

altimetry may well affect the results. The profiles of Figures 26 and 27 presented sufficient evidence that surveys over this kind of terrain may be conducted at higher and safer altitudes without serious loss in resolution. The 300-m flights of those figures were adapted from this study which is a more generalized study of the effects of altitude upon a standard resistivity survey.

The flightlines of the surveys discussed were given in Figure 17. The flightline spacing was narrowed to 0.16 km (mean value) to improve resolution. In Figure 28 are compared the resistivity contours of the two surveys. From these contours the following observations may be made:

1. All the major anomalies of the lower altitude repeat at the higher altitude except for the one between Gardner and Togue ponds. This 9000 ohm-m anomaly

at 150 m reduces to two smaller 5000 ohm-m anomalies at 300 m.

2. Not all the high resistivity anomalies at 150 m decrease in intensity at 300 m. The 8000 ohm-m anomaly between Gardner and Deboullie ponds increases to 10,000 ohm-m and two new 5000 ohm-m anomalies appear above (northeast of) Black Pond.

3. The contours over the ponds are generally of higher value at the 300-m level.

Figure 29 gives the normalized distributions of the digitized resistivity computations for all flightlines of both surveys. The normalized distribution of the 300-m survey is more concentrated about the mean value, which is very similar for both surveys, but has a much greater percentage – 19% vs 10% – of values between 4000 and 5000 ohm-m. This increase reflects the numerous 5000 ohm-m anomalies of the 300-m
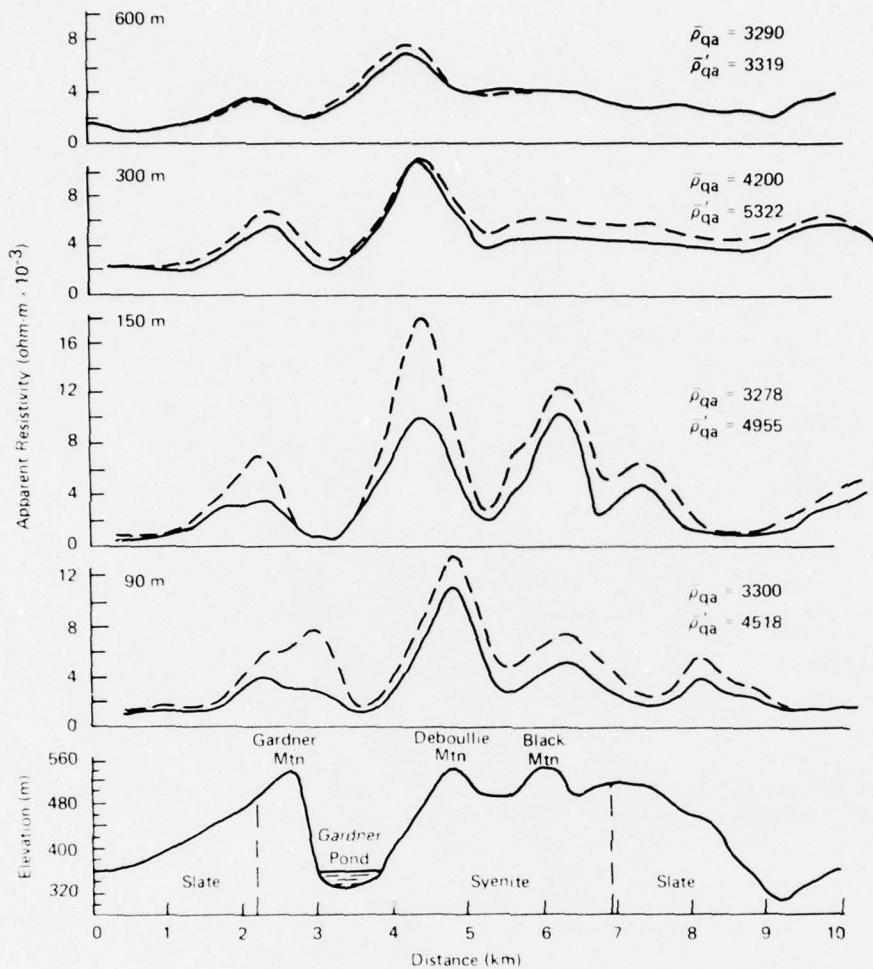
Figure 26. Standard (solid) and topographically corrected (broken) ρ_{qa} profiles for altitude series A. $\bar{\rho}_{qa}$ is the mean of the standard and $\bar{\rho}'_{qa}$ is the mean of the corrected profiles.

contours. The 300-m distribution also has a much smaller percentage — 3% vs 14% — of values below 1000 ohm-m which reflects a decrease in sensitivity to the low resistivity areas.

The results of both surveys are generally very similar, demonstrating that most resistivity information measured with a standard airborne wavetilt system over topographic relief this severe is preserved to at least a 300-m mean flight altitude. Also, for the 150-m standard survey, the many local changes experienced in flight altitude did not significantly affect the resistivity contours to be derived from the standard data processing method.

Study no. 4 – ground level study of phase and amplitude effects

Figures 30 and 31 are the profiles of ρ_{as} and ϕ_s along each traverse of Figure 18. These values were used to profile ρ_{qs} (derived from eq 17) in Figures 32 and 33 which will be compared to the airborne results in Figure 19 or 20. It is assumed that E_z and H_y are generally in phase, thereby making the comparisons valid. The ρ_{qs} profile values will be explained with reference to the data of Figures 30 and 31.

The ground traverses are described below. The parenthesized numbers after the traverse letters refer to the number of stations where measurements were

31
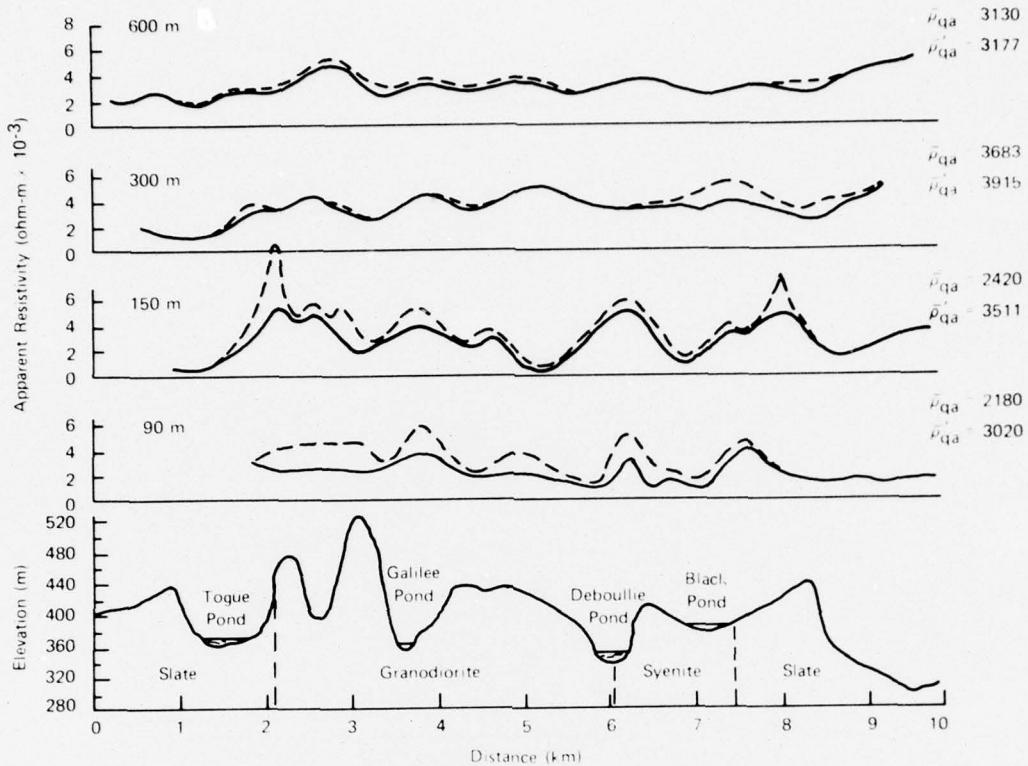
Figure 27. *Standard (solid) and topographically corrected (broken)* ρ_{qa} *profiles for altitude series B.* $\bar{\rho}$ *is the mean of the standard and* $\bar{\rho}'$ *is the mean of the corrected profiles.*

made. The subscript *s* refers to the ground (surface) value of a quantity

1. Traverse A-A' (12). This is predominantly under a 3000 ohm-m region of the airborne survey just above Togue Pond. $\bar{\rho}_{qs} = 1560$ ohm-m not including the measurements at the pond shore. The three measurements taken at the pond shore were very low at 350, 240 and 180 ohm-m.

2. Traverse B-B' (11). This is under the 5000 and 6000 ohm-m airborne contours north of Denny Pond in the granodiorite section. $\bar{\rho}_{as} = 4473$ ohm-m, $\bar{\phi}_s = 43.5°$ and $\bar{\rho}_{qs} = 3978$ ohm-m.

3. Traverse C-C' (11). This is under the 12,000 ohm-m anomaly west of Denny Pond in the granodiorite section. One value of ρ_{qs} exceeds 12,000 ohm-m but $\bar{\rho}_{qs}$ is much less at 5360 ohm-m. $\bar{\rho}_{as} = 11,545$ ohm-m which is very close to the peak airborne value, but $\bar{\phi}_s = 30.6°$ which explains the lower value for $\bar{\rho}_{qs}$.

4. Traverse D-D' (63). This runs the length of Togue Pond. It is generally under the 2000 and 3000

ohm-m airborne contours and $\bar{\rho}_{qs} = 1825$ ohm-m.

5. Traverse E-E' (41). This covers all three rock types as it passes up Gardner Mountain from south to north. In the granodiorite section it passes under an 8000 ohm-m airborne anomaly. Over the granodiorite, $\bar{\rho}_{as} = 9009$ ohm-m but $\bar{\rho}_{qs} = 4374$ ohm-m because $\bar{\phi}_s = 28.9°$. Over the syenite section, which is directly on the ridge of Gardner Mountain, the traverse is under 3000, 2000 and 1000 ohm-m airborne contours but $\bar{\rho}_{qs}$ is much greater at 6100 ohm-m.

6. Traverse F-F' (46). The first part of this traverse is over the slate and has a very low $\bar{\rho}_{qs} = 1646$ ohm-m because $\bar{\phi}_s = 16.9°$. Over the granodiorite, $\bar{\phi}_s$ increases to 35.9°, $\bar{\rho}_{as} = 7086$ ohm-m and $\bar{\rho}_{qs} = 4597$ ohm-m. Over this traverse the airborne contours are 3000, 4000 and 5000 ohm-m.

7. Traverse G-G' (13). This is over slate and goes up Whitman Mountain directly under an airborne 8000 ohm-m (actual peak value is 8900) anomaly. $\bar{\rho}_{qs} = 8503$ ohm-m and $\bar{\phi}_s$ is a relatively high 41°.

32

Figure 29. Normalized distributions of the digitized resistivity values for the 150-m and 300-m surveys.

$\bar{\rho}_{qa} = 3545$ ohm-m
1793 Samples

$\bar{\rho}_{qa} = 3291$ ohm-m
1646 Samples

Percent of Total

Resistivity Classes (10^3 ohm-m)

b. 300 m.

a. 150 m.

Figure 28. ρ_{qa} contours at 150-m and 300-m mean flight altitudes. Contour values are in thousands of ohm-meters; average flightline spacing is 0.16 km.

33

Figure 31. ρ_{as} (solid) and ϕ_s (broken) at 17.8 kHz along ground traverses F-F' through I-J' of Figure 18.
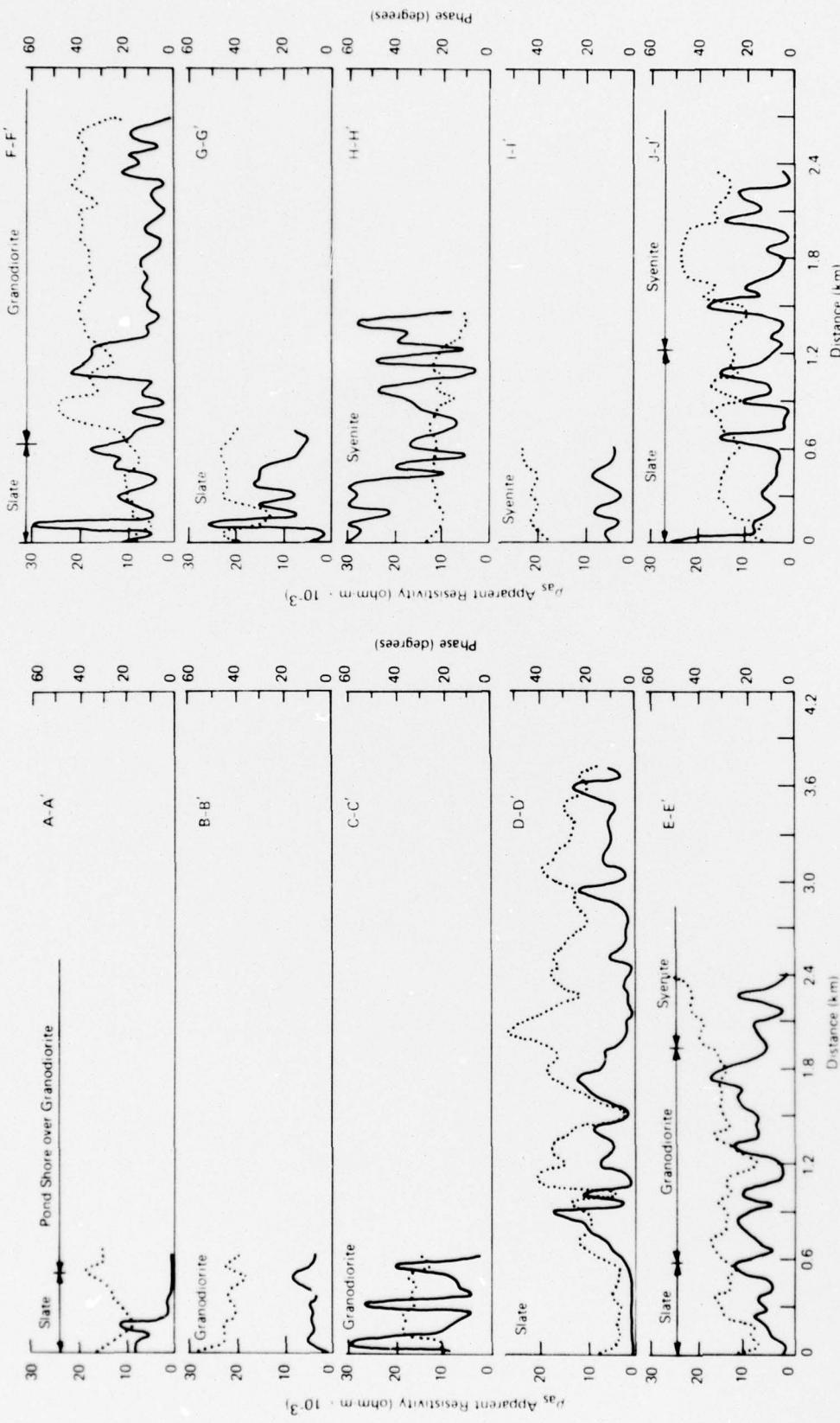
Figure 30. ρ_{as} (solid) and ϕ_s (broken) at 17.8 kHz along ground traverses A-A' through E-E' of Figure 18.

34

Figure 32. ρ_{qs} profiles at 17.8 kHz along ground traverses A-A' through E-E'.

35
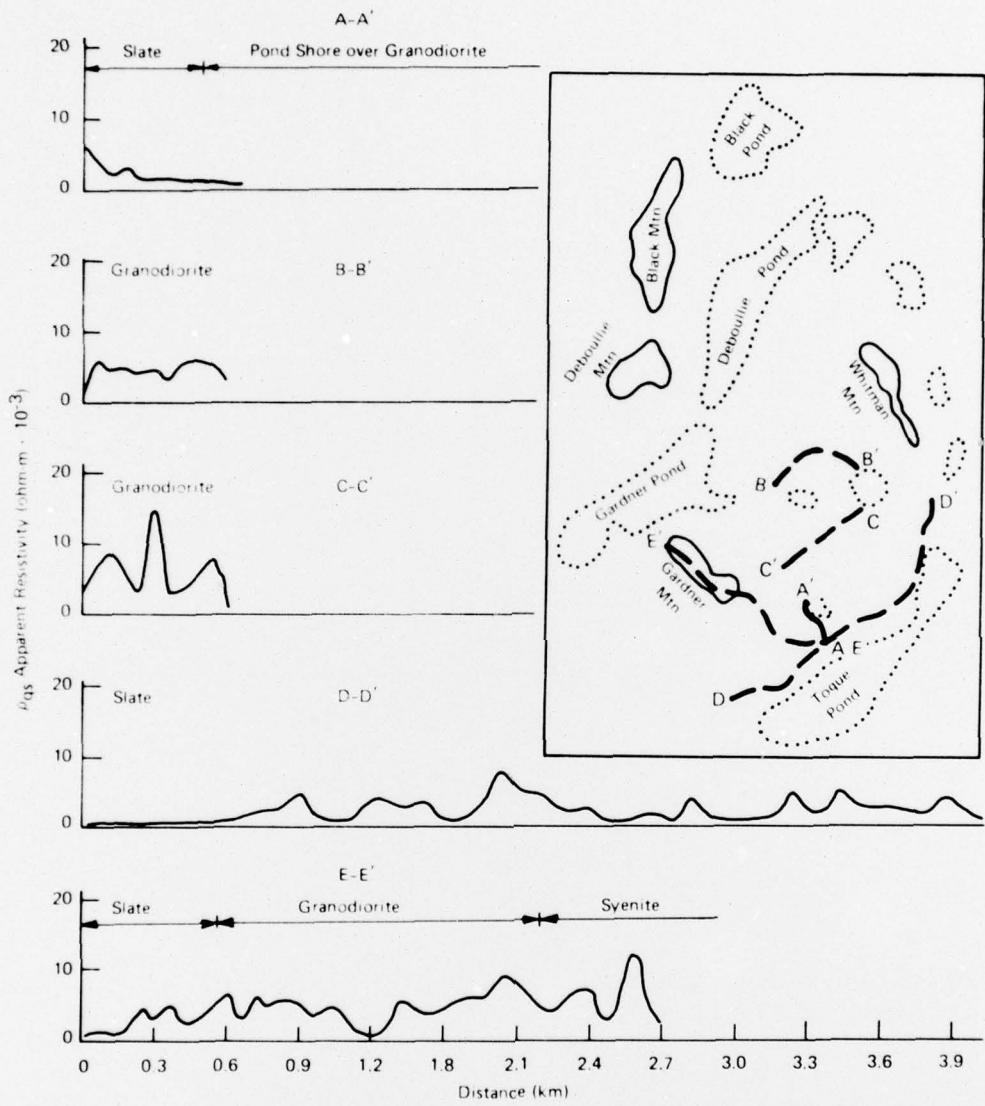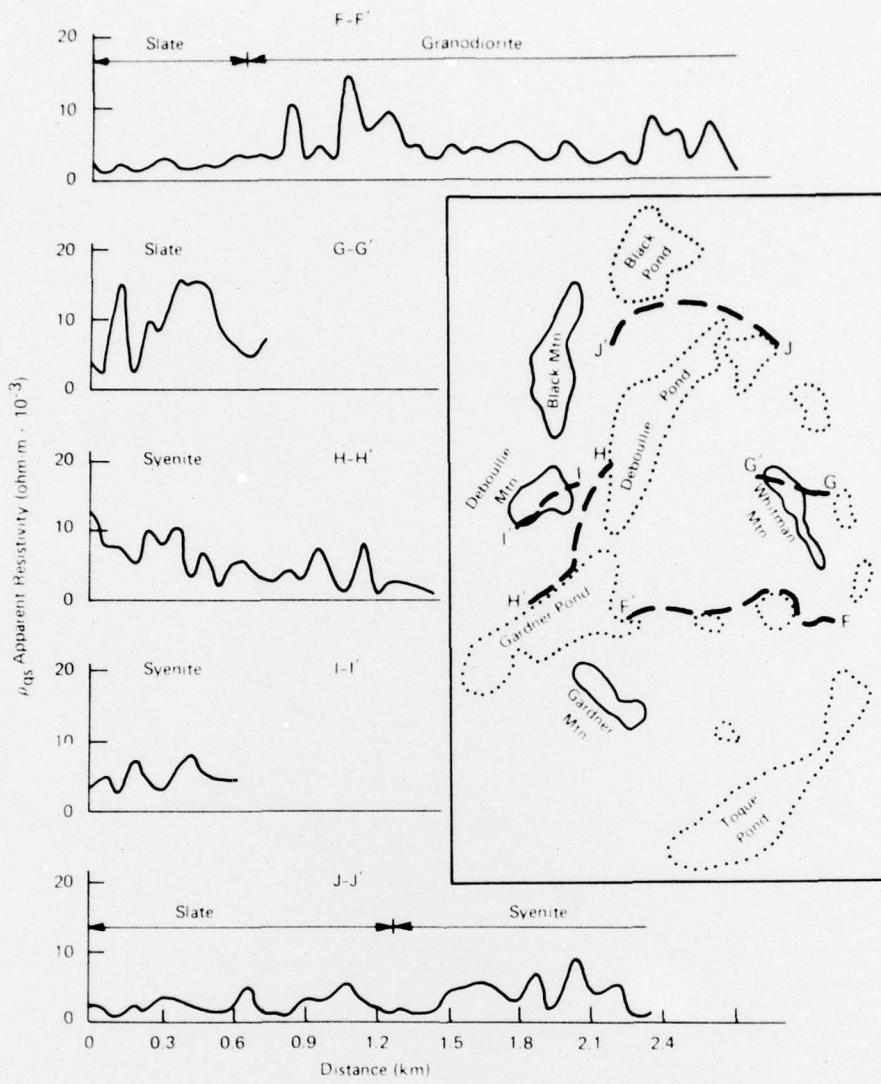
Figure 33. ρ_{qs} profiles at 17.8 kHz along ground traverses F-F' through J-J'.

8. Traverse H-H' (25). This is all over syenite and passes directly under the 10,000 ohm-m anomaly between Deboullie and Gardner ponds. As shown in Figure 31, four of these readings are indicated at 30,000 ohm-m, but they actually exceeded the calibrated range of the instrument and could not be determined. $\bar{\phi}_s$ was exceptionally low along this traverse at 21.4° with a standard deviation of only 22% for all 25 readings.

9. Traverse I-I' (11). This is directly across the twin peaks of Deboullie Mountain and at the edge of the syenite. The airborne contours indicate values between 1000 and 3000 ohm-m but $\bar{\rho}_{qs}$ is much higher at 4685 ohm-m. $\bar{\phi}_s$ is high at 42°.

10. Traverse J-J' (40). This traverse passes from slate to syenite and stays under a 3000 ohm-m contour. This corresponds well with $\bar{\rho}_{qs}$ = 2480 ohm-m for the slate and $\bar{\rho}_{qs}$ = 3492 ohm-m for the syenite.

Phase angles near 45° do occur, such as on the east flank of Whitman Mountain and over the ridges of Gardner and Deboullie mountains. Most usually, however, they are between 20° and 35° for all rock types. At only 15 of the 270 ground stations is phase ever greater than 45°, and the average of these 15 readings is 48.7°.

In some cases the correlation of ρ_{qa} with ρ_{qs} is excellent as with traverses G-G' and J-J'. The syenite section of traverse E-E' and all of I-I' are directly over

36

Syenite, 64 samples
$\bar{\rho}_{as}$ = 10647

Syenite
$\bar{\phi}_s$ = 31.5

Granodiorite, 79 samples
$\bar{\rho}_{as}$ = 7885

Granodiorite
$\bar{\phi}_s$ = 34.2

Slate, 127 samples
$\bar{\rho}_{as}$ = 6276

Slate
$\bar{\phi}_s$ = 26.1

Normalized Distribution (%)

Apparent Resistivity Classes (10^3 ohm-m)

Phase (Deg)
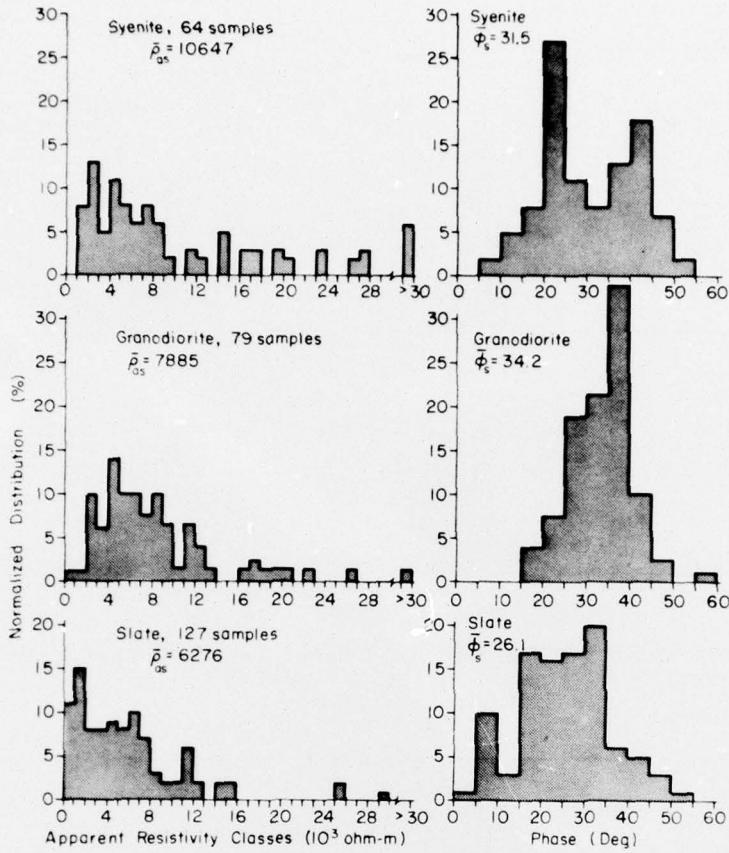
Figure 34. Normalized distributions and means of the ground values ρ_{as} and ϕ_s.

ridges where E_z is suppressed. Correspondingly, $\bar{\rho}_{qs}$ is well above $\bar{\rho}_{qa}$. In the cases of traverses C-C' and H-H' the ground readings are much lower than the highest airborne reading made over the same area.

Figure 34 gives the normalized distributions and means of the ground readings organized according to rock type. Generally, all three types have similar ρ_{as} distributions, with 67% of the syenite values, 75% of the granodiorite values and 70% of the slate values falling between 1 and 10,000 ohm-m. The syenite has the highest $\bar{\rho}_{as}$ followed by the granodiorite. The slate is almost as resistive as the granodiorite and far more resistive than the airborne readings indicate. Since only 13 of the 127 slate readings were taken under high airborne anomalies (all on Whitman Mountain), there is no bias in the slate data for these areas.

The phase distributions of Figure 34 show more discrimination among the rock types than do the ρ_{as} distributions. The syenite has two definite peaks, one between 20° and 25° and another between 40°

and 45°. The former is mostly due to flank readings and the latter to ridge readings. Only 19% of the syenite readings are within ± 5° of the mean. The granodiorite has a single strong peak between 35° and 40°, and 55% of the readings are within ± 5° of the mean. The slate has no distinct peaks above 10% and has the lowest mean. Forty-seven percent of all slate phases fall below 25° as opposed to only 11.5% for the granodiorite, which has a comparable ρ_{as} distribution.

Figure 35 compares the distributions of ρ_{qs} and ρ_{qa}. For all rock types the phase has significantly lowered the ground resistivities so that the three ground distributions are all comparable to those of the airborne. No values now appear above 16,000 ohm-m for the ground values. In all cases $\bar{\rho}_{qa}$ is much closer to $\bar{\rho}_{qs}$ than it is to $\bar{\rho}_{as}$. Eighty-one percent of all airborne slate values are below 3000 ohm-m; this compares favorably with 71% for the ground values. Seventy-three percent of all airborne granodiorite values are between 2000 and 6000 ohm-m, again comparing

37
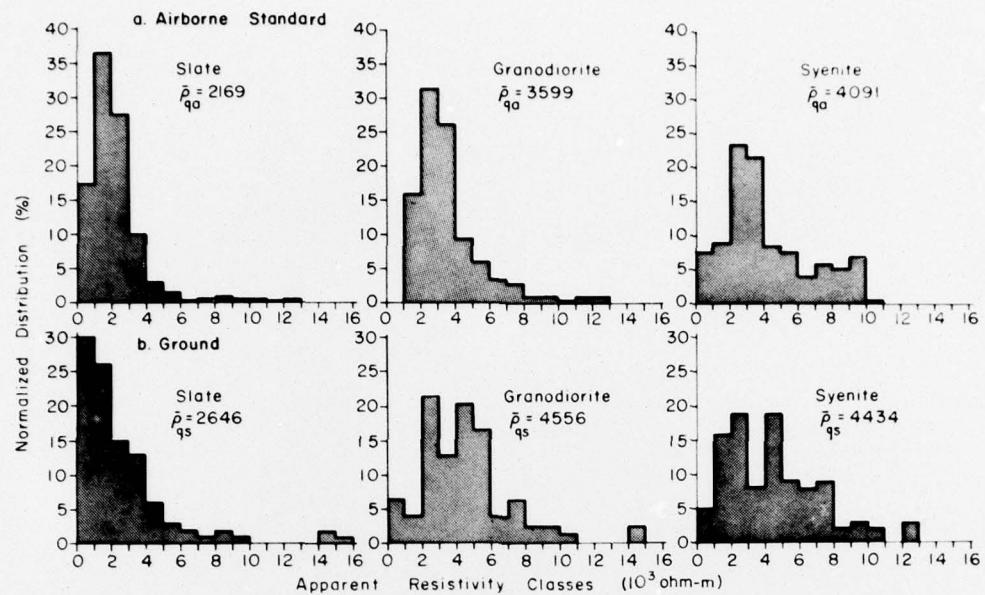
Figure 35. Comparison between the normalized distributions and means of the standard airborne and ground surveys of ρ_q.
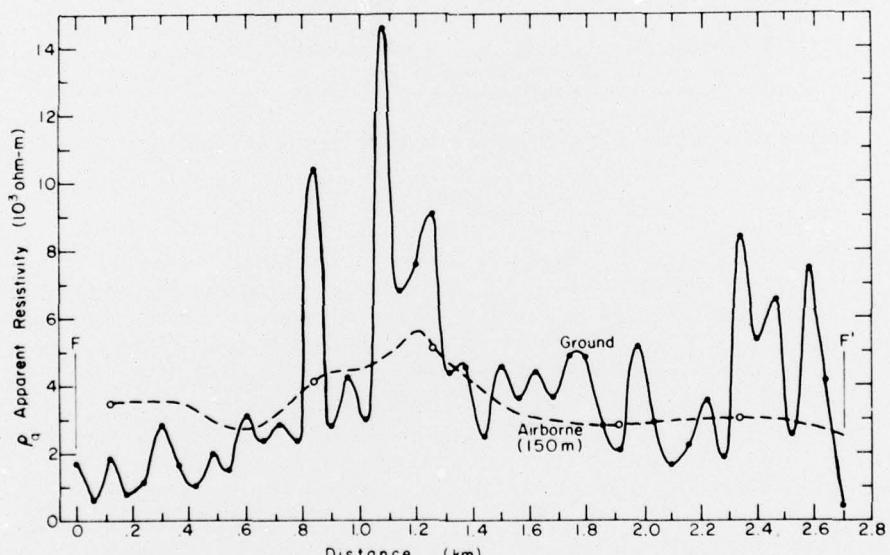
a. Airborne and ground values.

Figure 36. Comparison of airborne contoured values and ground readings of ρ_q for traverse F-F'. Dots and circles are actual measurements.
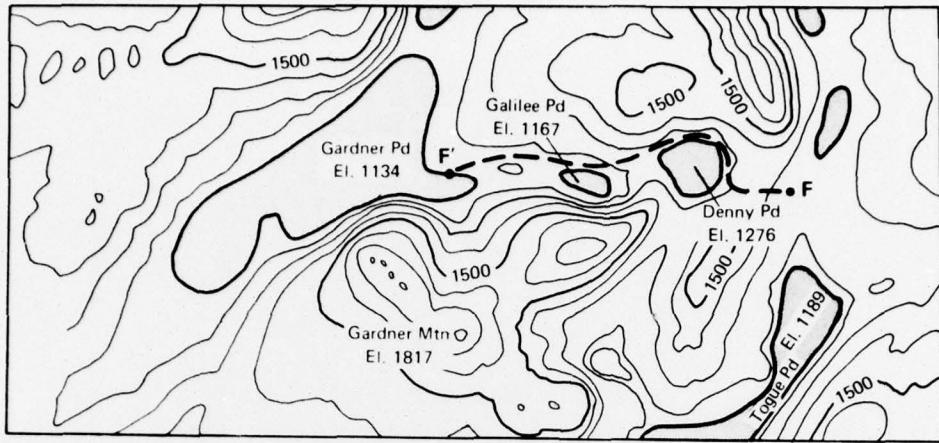
b. Location of traverse.

Figure 36 (cont'd).

favorably with 71.5% of the ground values. For the syenite, 61% of all values fall between 2000 and 6000 ohm-m for the airborne survey, compared to 55% for the ground survey. The mean ground values given for each rock type are slightly higher than the airborne values and this is probably due, in part, to the topographic enhancement of E_z discussed previously. Later, when topographic effects are eliminated and the standard survey is reevaluated, some of these comparisons between the means will improve.

Over regions where topography did not seriously disturb the airborne results, specific comparisons between ground and airborne values may be made to approximately determine the necessary size of a resistivity anomaly for airborne detection by contouring.

In Figures 36 and 37 are compared ρ_{qs} along traverses F-F′ and J-J′ with the overhead 150-m contoured values of ρ_{qa}. Points and circles on the curves indicate actual measurements. In Figure 36 an intense ground anomaly (peak value - 14,600 ohm-m) exists for a length of about 300 m and is interpreted by the airborne contouring as a 5500-ohm-m anomaly. To the right, a lesser ground anomaly (peak value = 8400 ohm-m) also occurs for a length of about 300 m but is barely detected by the contouring. In Figure 37 one large ground anomaly (peak value = 9000 ohm-m) occurs at the right for slightly more than 300 m and is discerned by the contouring. In both figures, ground anomalies of shorter length are hardly seen at altitude. Apparently 300 m is near the significant physical
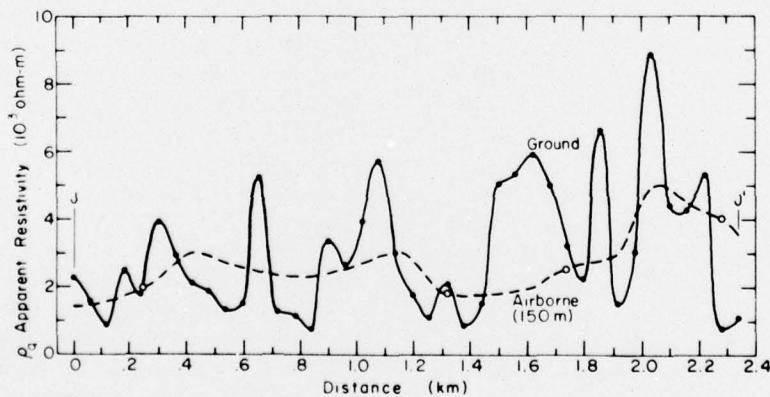
a. Airborne and ground values.

Figure 37. Comparison between airborne contoured values and ground readings of ρ_q for traverse J-J′. Dots and circles are actual measurements.

39
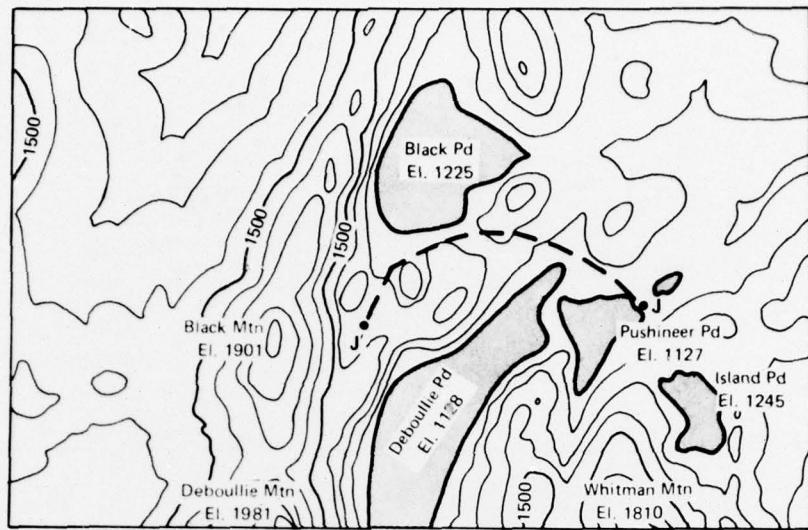
b. Location of traverse.

Figure 37 (cont'd). Comparison between airborne contoured values and ground readings of ρ_q for traverse J-J'. Dots and circles are actual measurements.

dimension which ground anomalies of these intensities (above background levels of 3000 to 4000 ohm-m) must have to register as an airborne anomaly at 150-m altitude and approximately 400-m flightline spacing. This approximate size corresponds to the – 10 db sensitivity width of an airborne dipole at 150-m altitude.

THE STANDARD SURVEY REEVALUATED

The studies of flight series A and B in *Results* revealed that only E_{zi} is disturbed by topographic relief while E_{xq} contains the actual resistivity information. The behavior of E_{zi} supports the earlier observations of Harrison (1971), discussed previously. The ground-air comparisons of ρ_q over mountain ridges (traverses E-E' and I-I') demonstrated that ρ_{qa} is suppressed in these settings by this effect.

Along each flightline (Fig. 15) of the standard survey, E_{zi} responds to the topographic relief in the same manner of Figures 22 and 23. Over each mountain ridge, E_{zi} rises. Over the flatter sections, such as the ponds, all the E_{zi} levels are within a few percent of each other as was evident in Figures 22 and 23. Therefore, at each fiducial mark, a new apparent resistivity ρ'_{qa} was computed by adjusting E_{zi} along an entire flightline to the field level above these flat sections. The formula for ρ'_{qa} is

$$\rho'_{qa} = \rho_{qa} \, (E_{zi}/E_0)^2 \qquad (23)$$

where $\qquad (23)$

$$\rho_{qa} = (2/\omega\epsilon_0) \, (E_{xq}/E_{zi})^2$$

as before and E_0 is the value of E_{zi} over the flat areas, such as the ponds. This undisturbed level is not necessarily the minimum level. Often E_{zi} dips slightly below the undisturbed level on both sides of the peak response to a topographic disturbance.

Figure 38 presents this reevaluation of the standard survey. The locations of the high resistivity patterns are similar to those of Figure 19 but several features have been changed:

1. One anomaly of Figure 19 is considerably more intense, having risen from 10,000 to 17,000 ohm-m. This lies on a flank between Deboullie and Gardner ponds and also occurs where several ground readings could not be determined because they exceeded 30,000 ohm-m.

2. The anomaly over Gardner Mountain has now become three anomalies that include the entire mountain. Above the syenite section, the ρ_{qa} contours have risen from 1000-3000 ohm-m in Figure 19 to 6000 and 7000 ohm-m in Figure 38. This agrees better with the value $\bar{\rho}_{qs}$ of 5342 ohm-m for eight ground readings along this ridge, and the corrected values along a section of flightline no. 9 over Gardner Mountain are shown in Figure 39.

40
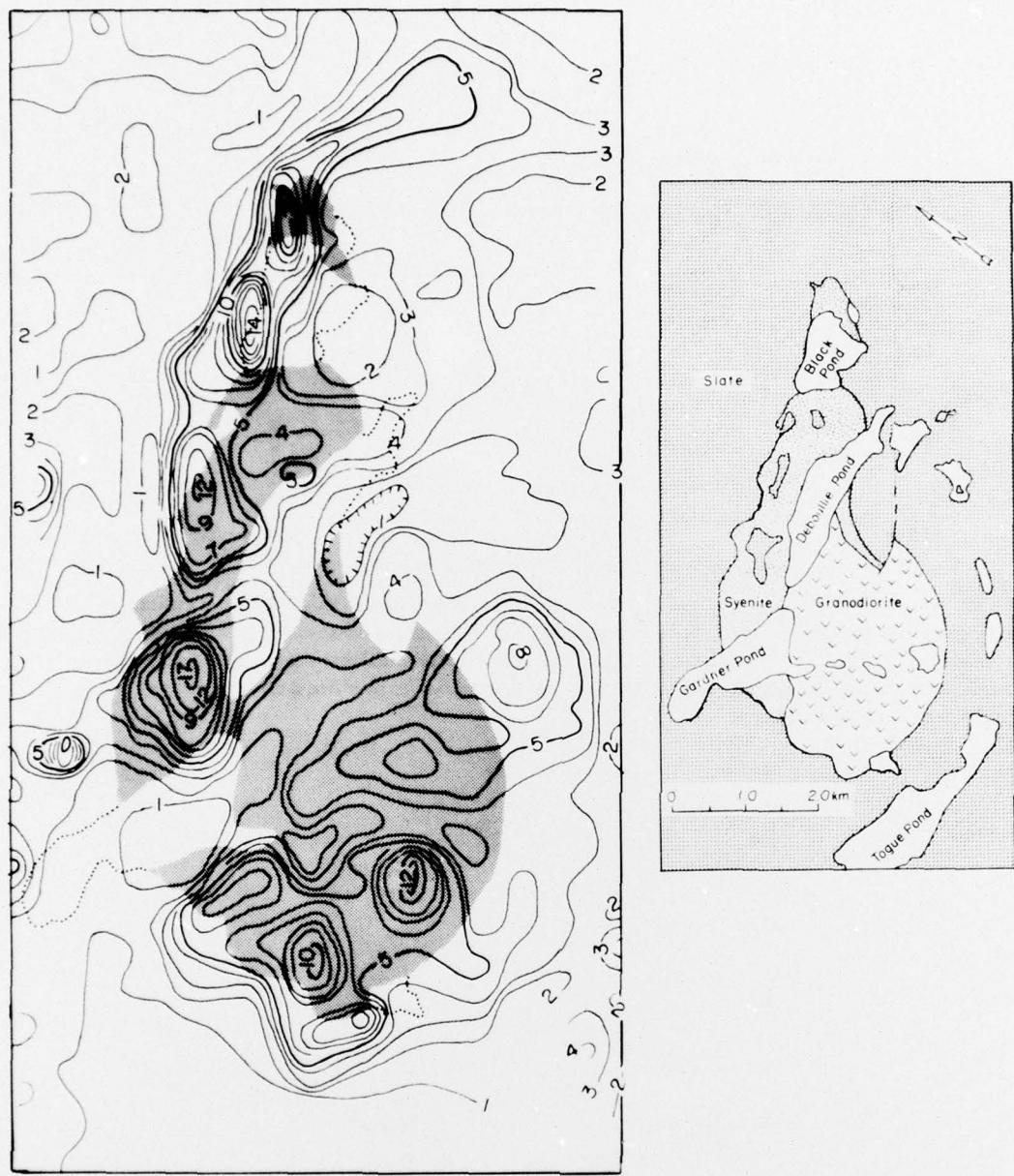
Figure 38. Apparent resistivity contours of the topographically corrected standard survey superimposed upon the geology. Shaded areas are syenite and granodiorite. Contour values are to be multiplied by 1,000. Mean flight altitude = 150 m.

3. Between the twin peaks of Deboullie Mountain (northern boundary of the syenite section), the airborne contours have risen from 1000-2000 ohm-m in Figure 19 to 3000-5000 ohm-m. This agrees well with the value $\bar{\rho}_{qs}$ = 4685 ohm-m for 11 ground readings along this ridge.

4. The anomaly over Whitman Mountain in the slate section has marginally decreased from 8900 ohm-m to 8100 ohm-m. This is also in good agreement with the value $\bar{\rho}_{qs}$ = 8500 ohm-m for 13 readings across the southern flank.
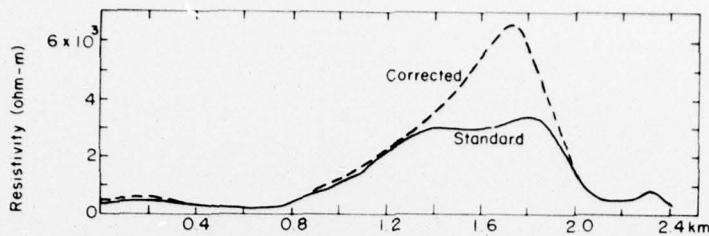
a. Comparison of standard and corrected ρ_q values for flightline 9.
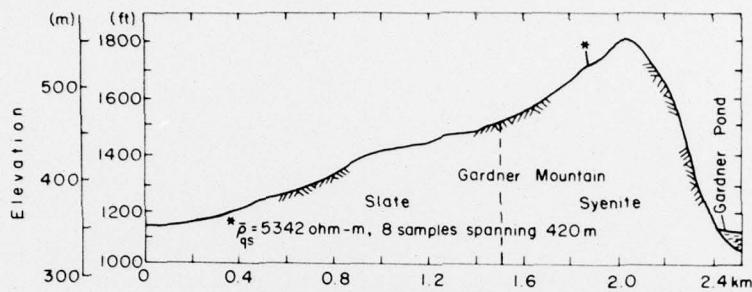
b. Topographic and geologic profile beneath flightline.

Figure 39. Apparent resistivities ρ_{qa} and ρ'_{qa} computed along flightline no. 9 over Gardner Mountain and topographic and geologic profile beneath the flightline. The eight ground samples in (b) were made linearly in a direction transverse to the flightline. The corrected values over the syenite are more consistent with the ground readings and with other airborne anomalies over the syenite regions of Deboullie and Black mountains.
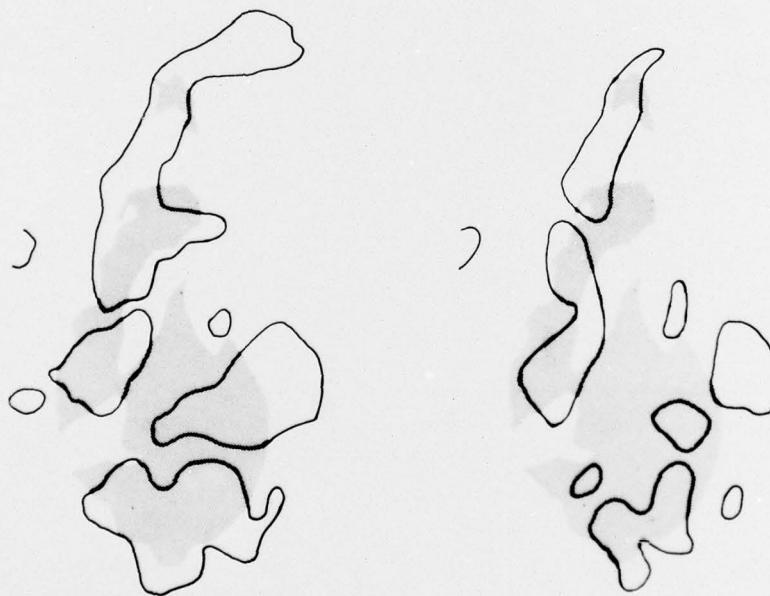
a. 4000 ohm-m contour corrected survey.   b. 4000 ohm-m standard.

Figure 40. Comparison between the igneous areas encompassed by the 4000 ohm-m contours of the topographically corrected survey (a) and the standard survey (b). The shaded regions cover the igneous geology.

42

a. Airborne Corrected

Slate $\bar{\rho}'_{qa} = 2687$

Granodiorite $\bar{\rho}'_{qa} = 4767$

Syenite $\bar{\rho}'_{qa} = 6038$

b. Ground

Slate $\bar{\rho}_{qs} = 2646$

Granodiorite $\bar{\rho}_{qs} = 4556$

Syenite $\bar{\rho}_{qs} = 4434$

Normalized Distribution (%)

Apparent Resistivity Classes (10^3 ohm-m)
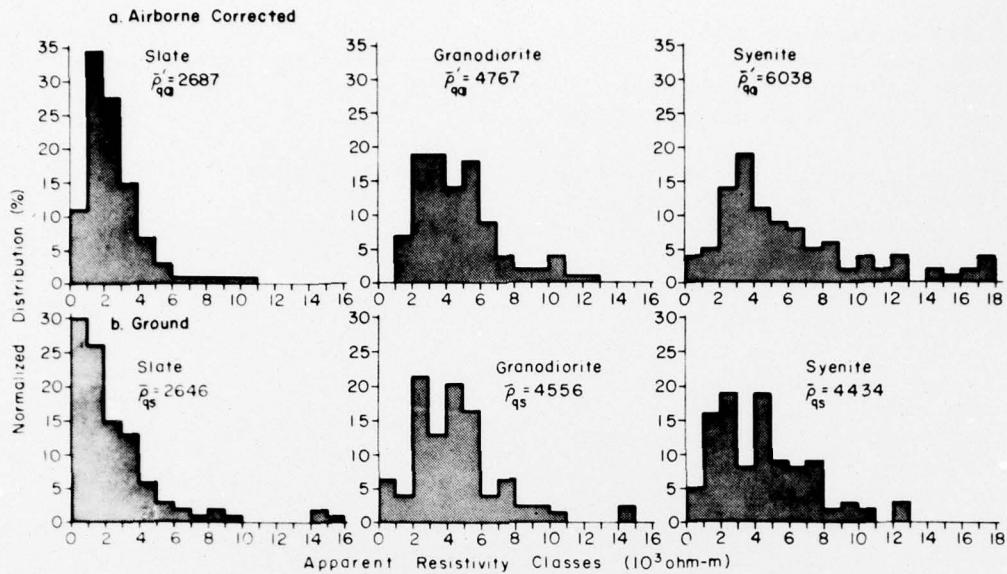
Figure 41. Comparison between the normalized distributions and means of the topographically corrected airborne survey of ρ'_{qa} and the ground survey of ρ_{qs}.

5. In the top portion of the figure, 4000 and 5000 ohm-m contours now appear as they did in the 300-m survey of Figure 28 but not in the 150-m survey of Figures 19 or 28.

6. A new anomaly has occurred in the slate section on the western approach to Deboullie Mountain. No ground readings were made to verify this.

A more general comparison between the standard and the corrected survey is made in Figure 40. In this figure, the areas encompassed by the 4000 ohm-m contour are compared. This contour value was chosen because it is just below $\bar{\rho}_{qs}$ for both igneous rock types but well above $\bar{\rho}_{qs}$ of the slate values. Therefore, this contour might be expected to best define the limits of the igneous geology. As shown in the comparison, the topographically corrected contours contain much more of the igneous geology in all sections of the map. Only at the very top of the figure is this contour overextended in relation to the uncorrected standard survey.

The normalized distributions of resistivity values for the reevaluated survey are given in Figure 41. The comparisons are similar to those of Figure 35 where similar comparisons were made with the standard airborne results. In this case, however, the mean values for the slate and granodiorite have drawn closer to those of the ground measurements, although $\bar{\rho}'_{qa}$ for syenite has increased to over 6000 ohm-m.

CONCLUSIONS AND FINAL REMARKS

Important conclusions to be drawn from these VLF resistivity studies are as follows:

1. Above ridges and peaks E_{zi} was always enhanced in the manner predicted by the theories of Harrison et al. (1971) for electrostatic dipole models of mountains. As verified by ground measurements, this effect reduced the apparent resistivity (as measured with standard airborne procedures) above these locations and caused the higher resistivity zones to be concentrated strictly on mountain flanks.

2. The high altitude flights showed that resistivity predominantly affects E_{xq}, while E_{zi} is relatively unaffected by resistivity.

3. Most resistivity information was preserved to at least 300-m altitude when the resistivity was computed from the actual E_{zi} and E_{xq} using standard procedures. This resulted from the compensation for the amplitude loss in E_{xq} by the amplitude loss in E_{zi} over mountainous regions.

4. Geologic resolution improved when the airborne apparent resistivity was recomputed using the topographically corrected E_{zi}.

5. Wavetilt and surface impedance phase were generally similar, as deduced from the correlation of ground and airborne ρ_q values. This implies that E_z and H_y were also generally in phase.

6. The phase of the wavetilt was an important factor

43

for distinguishing high resistivity areas in regions of near surface, crystalline bedrock.

7. Resistivity anomalies less than approximately twice the survey altitude in dimension were difficult to detect.

Recordings of E_{xi} were also made but were highly erratic. This behavior was expected from the coupling of E_{zi} into the horizontal dipole during aircraft roll but was also probably due to topographic scattering. Topographic scattering is the primary reason why antenna stabilization schemes designed to measure the full wavetilt cannot work: the in-phase component of the wavetilt is more than likely destroyed before it can be measured by an airborne antenna. The phase of surface impedance correlates with wavetilt phase only as determined by E_{xq} and E_{xi} before scattering. It seems probable, however, that E_{xi} at ground level is a meaningful quantity because so many phase measurements were between $20°$ and $35°$, which is plausible for the geology encountered.

The observed phase angles of less than $45°$ are probably due, in a general sense, to a combination of the two factors: 1) a stratification in resistivity such as would be caused by a gradation in weathering with depth, and 2) high permittivity values, especially for the slate for which values as high as 34 have been reported by Parkomenkho (1967). The latter factor would imply that, even at VLF, crystalline rock distinctions could have actually been made on the basis of relative permittivity. If permittivity were a factor, then some of these results might be different if another transmitter located in a direction orthogonal to the direction of Cutler, Maine, had been monitored. This is because slate can be anisotropic due to its cleavage. A study using orthogonal transmitters in such an area might then define surface impedance tensors from which additional geologic information might possibly be uncovered.

The theoretical basis of this exploration method demands infinite layers of homogeneous material in order to correlate the field ratios with the resistivity. At the area studied, the largest horizontal dimension of the igneous region was less than half of the wavelength (16.8 km at 17.8 kHz) monitored. Therefore, it might seem improbable that field measurements processed on the basis of a theory that can be derived from geometric optics should provide results consistent with values determined by more conventional field and laboratory techniques. Nevertheless, these studies present observational evidence that ground waves can rapidly recover* (in terms of fractions of a wavelength)

---
*Reference to the theory of the "recovery" effect was given in *Irregular surface and subsurface conditions*.

the desired relative electromagnetic field strengths and phases when passing from one resistivity condition to another.

LITERATURE CITED

Alpert, Y.A. (1963) *Radio wave propagation and the iono-sphere*. New York: Consultants Bureau, Translated from Russian.

Barringer, A.R. (1972, 1973) Geophysical exploration method using the vertical electric component of a VLF field as a reference. Canadian Patent no. 1,261,732; USA Patent no. 3,594,633 and 3,763,419.

Blomquist, A. (1970) Equipment for in-situ measurement of the dielectric properties of ground and ice. *Proceedings of the International Meeting on Radio Glaciology*, Lyngby, Denmark, p. 54-70.

Boone, G. (1962) Potassic feldspar enrichment in magma: origin of syenite in Deboullie district, northern Maine. *Geological Society of America Bulletin*, vol. 73, p. 1451-1476.

Cagniard, L. (1953) Basic theory of the magneto-telluric method of geophysical prospecting. *Geophysics*, vol. 18, no. 3, p. 605-635.

Coggon, J.H. (1971) Electromagnetic and electrical modeling by the finite element method. *Geophysics*, vol. 36, p. 132-155.

Collett, L.S. and Becker, A. (1967) Radiohm method for earth resistivity surveying. Canadian Patent no. 795919.

Culley, R.W., F.L. Jagodits, and R.E. Middleton (1975) E-phase system for detection of buried granular deposits. Paper presented at the *Symposium on Modern Innovations in Subsurface Exploration*. University of Toronto, Toronto, Canada.

Eliassen, K.E. (1957) A survey of ground conductivity and dielectric constant in Norway within the frequency range 0.2-10 mc. *Geofysiske Publikasjoner* (Oslo), vol. 19, no. 11, p. 1-30.

Frischknecht, F.C. (1973) Electromagnetic scale model studies of geophysical methods using a plane wave source. University of Colorado, Ph.D. Thesis (unpublished).

Geological Survey of Canada (1973) Geophysical survey map of the Tuktovaktuk Region, Canadian NWT. Open file report no. 220. Map available from the Canadian Geological Survey, Dept. of Energy, Mines and Resources, Ottawa, Canada, N.T.I.S. Reference 107c/8.

Grim, R.E. (1953) *Clay mineralogy*. New York: McGraw Hill Book Co., Inc.

Harrison, R.P., J.L. Hecksher, and E.A. Lewis (1971) Helicopter observations of very low frequency waves over certain mountains and shorelines. *Journal of Atmospheric and Terrestrial Physics*, vol. 33, p. 101-110.

Hoekstra, P., P.V. Sellmann, and A.J. Delaney (1974) Airborne resistivity mapping of permafrost near Fairbanks, Alaska. CRREL Research Report 324, AD A000694.

Hoekstra, P., P.V. Sellmann, and A.J. Delaney (1975) Ground and airborne resistivity surveys of permafrost near Fairbanks, Alaska. *Geophysics*, vol. 40, no. 4, p. 641-656.

Hollingworth, J. (1926) The propagation of radio waves. *Journal of the Institute of Electrical Engineers*, vol. 46, p. 579-595.

Hughes, W.J. and J.R. Wait (1975) Effective wavetilt and surface impedance over a laterally inhomogeneous two-layer earth. *Radio Science*, vol. 10, no. 11, p. 1001-1008.

Jones, F.W. and A.T. Price (1970) The perturbations of alternating geomagnetic fields by conductivity anomalies. *Geophysical Journal of the Royal Astronomical Society*, vol. 20, p. 317-334.

Jordan, E.C. and K.G. Balmain (1968) *Electromagnetic waves and radiating systems*, 2nd edition. Englewood Cliffs, New Jersey: Prentice-Hall, Inc.

Keller, G.V. and F.C. Frischknecht (1966) *Electrical methods in geophysical prospecting*. New York: Pergamon Press.

Keller, G.V., A.B. Level, and F.L. Avsman (1970) Evaluation of airborne electromagnetic surveying for mapping variations in rock strength. Colorado School of Mines, Air Force Cambridge Research Laboratories, Contract Report no. F19628-69-C-0281.

King, R.J. (1968) Crossed dipole method of measuring wavetilt. *Radio Science*, vol. 3, no. 4, p. 345.

Kraichman, M.B. (1970) Handbook of electromagnetic propagation in conducting media. Headquarters, U.S. Naval Materiel Command, Washington, D.C., U.S. Government Printing Office.

Lytle, R.J. (1975) Theory relating to remote electromagnetic probing of a non-uniform coal seam. Lawrence Livermore Laboratory, Livermore, California, UCRL-51799.

McKim, H.L. and C.J. Merry (1975) Use of remote sensing to quantify construction material and to define geologic lineations: Dickey-Lincoln School Project, Maine. CRREL Special Report 242, AD A023276.

McNeill, J.D., F.L. Jagodits, and R.S. Middleton (1973) Theory and application of the E-Phase airborne resistivity method. *Proceedings of the Symposium on Exploration Electromagnetic Methods*, Toronto, University of Toronto.

Nabetani, S. and D. Rankin (1969) An inverse method of magnetotelluric analysis for a multi-layered earth. *Geophysics*, vol. 34, p. 75-86.

Norton, K.A. (1936) The propagation of radiowaves over the surface of the earth and in the upper atmosphere. *Proceedings of the Institute of Radio Engineers*, vol. 24, p. 1367-1387.

Paal, G. (1965) Ore prospecting based on VLF-radio signals. *Geoexploration*, vol. 3, no. 3 p. 139-147.

Paal, G. (1968) Very low frequency measurements in northern Sweden. *Geoexploration*, vol. 6, p. 141-149.

Palacky, G.J. and F.L. Jagodits (1975) Computer data processing and quantitative interpretation of airborne resistivity surveys. *Geophysics*, vol. 40, no. 5, p. 818-830.

Parkomenkho, E.I. (1967) *Electrical properties of rock*. Translated from Russian by G.V. Keller, New York: Plenum Press.

Parrot, W.H. and W.M. Fleming (1970) The temperature structure of a mid-latitude, dimictic lake during freezing, ice cover and thawing. CRREL Research Report 291, AD 715716.

Sellmann, P.V., P. Hoekstra, and A. Delaney (1974) Airborne resistivity survey: An aid in bedrock geology reconnaissance. CRREL Special Report 202, AD 777792.

Sellmann, P.V., A.J. Delaney, and P. Hoekstra (1975) Radio-wave resistivity measurements in northern Maine for identifying bedrock type. CRREL Special Report 238, AD 017944.

Sommerfeld, A. (1909) Über die Ausbreitung der Wellen in der drahtlosen Telegraphic. *Annalen der Physik*, vol. 28, p. 665.

Swift, C.M. (1971) Theoretical magnetotelluric and terrain response from two-dimensional inhomogeneities. *Geophysics*, vol. 36, p. 38-52.

Telford, W.M., L.P. Geldart, R.E. Sheriff, and D.A. Keys (1976) *Applied geophysics*. Cambridge: Cambridge University Press.

Wait, J.R. (1962) *Electromagnetic waves in stratified media*. New York: Pergamon Press.

Wait, J.R. (editor) (1971) *Electromagnetic probing in geophysics*. Boulder, Colorado: Golem Press.

Ward, S.H. (1967) Electrical methods. In *Mining Geophysics*, vol. II, *Theory*, Society of Exploration Geophysicists, Tulsa, Oklahoma.

Watt, A.D. (1967) *VLF radio engineering*. New York: Pergamon Press.

Weyl, H. (1919) Ausbreitung elektromagnetischer Wellen über einem ebenen Leiter. *Annalen der Physik*, vol. 60, p. 481-500.

APPENDIX: GLOSSARY OF GEOLOGIC TERMS USED
(adapted from *Glossary of Geology* by the
American Geological Institute, Washington, D.C.)

Basalt A dark to medium-dark, commonly volcanic, igneous rock.

Chalk A soft, pure, fine-textured usually white to light gray or buff limestone of marine origin, consisting mainly of calcite.

Clay A loose, earthy, natural sediment or soft rock composed primarily of clay-size ($< 1/256$ mm) particles and characterized by high plasticity and mostly hydrous aluminum silicates.

Cleavage The property or tendency of a rock to split along secondary, aligned fractures or other closely spaced, planar structures or textures, produced by deformation or metamorphism.

Crystalline A descriptive term referring to a rock consisting wholly of crystals or fragments of crystals, e.g. an igneous rock lacking *glassy* material, or a metamorphic rock.

Dip The angle that a structural surface, e.g. a bedding or fault plane, makes with the horizontal, measured perpendicular to *strike* of the structure.

Ferromagnesian Containing iron and magnesium.

Foliation A general term for a planar arrangement of textural or structural features in any type of rock, e.g. cleavage in slate or schistosity in schist.

Glassy A descriptive term referring usually to the texture or luster of usually a volcanic rock. Glassy properties result from rapid cooling without distinct crystallization.

Gneiss A foliated metamorphic rock in which bands of granular minerals alternate with bands of flaky minerals.

Granite A term loosely applied to any light-colored, coarse grained igneous rock. Specifically, it refers to a definite composition of quartz, feldspar and ferromagnesian minerals.

Granodiorite A type of granitic rock of specified composition of quartz, feldspar and ferromagnesian minerals.

Igneous A descriptive term referring to a rock or mineral that solidified from a molten (magmatic) or partly molten material.

Intrusive A descriptive term usually referring to an igneous rock that has solidified from a magma emplaced in other rock structures.

Limestone A sedimentary rock consisting chiefly of calcium carbonate.

Loam A rich, permeable soil of similar proportions of clay, silt, sand and organic matter. Sometimes called topsoil.

Marl A term loosely applied to unconsolidated materials consisting chiefly of clay and calcium carbonate.

Metamorphic A descriptive term applied to a rock derived from pre-existing rock by mineralogical, chemical, and structural changes in response primarily to marked changes in temperature and pressure.

Permafrost Any material in which a temperature below $0°C$ has existed continuously for more than about two years. The definition is based exclusively on temperature.

Sandstone A sedimentary rock of sand size particles set in a silty or clayey matrix and cemented usually by silica, iron oxide or calcium carbonate.

Schist A strongly foliated metamorphic rock which can be readily split into thin flakes or slabs; i.e. it demonstrates the property of schistosity which is a type of cleavage.

Slate A fine-grained metamorphic rock that cleaves along planes independent of the original bedding.

47

Stock An igneous intrusion less than about 40 miles^2 in surface exposure.

Strike The direction or trend that a structural surface, e.g. a bedding or fault plane, takes as it intersects the horizontal.

Syenite An igneous rock similar to granite but of less quartz content.

Till Unsorted, unstratified and unconsolidated mixture of clay, sand and gravel. Till is usually of glacial origin.

Cover: View from southeast flank of Gardner Mountain, Maine. (Photograph by Steven Arcone.)